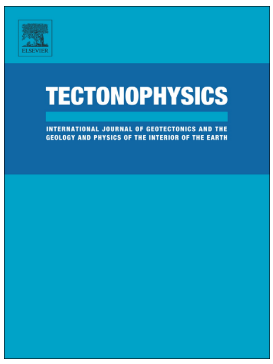

Sediment-starved trenches and rough subducting plates are conducive to tsunami earthquakes

Jacob Geersen

PII: S0040-1951(19)30148-9
DOI: https://doi.org/10.1016/j.tecto.2019.04.024
Reference: TECTO 128096

To appear in: *Tectonophysics*

Received date: 27 November 2018
Revised date: 8 March 2019
Accepted date: 23 April 2019

Please cite this article as: J. Geersen, Sediment-starved trenches and rough subducting plates are conducive to tsunami earthquakes, Tectonophysics, https://doi.org/10.1016/j.tecto.2019.04.024

Sediment-starved trenches and rough subducting plates are conducive to tsunami earthquakes

Jacob Geersen

GEOMAR Helmholtz Centre for Ocean Research Kiel, Wischhofstr. 1-3, 24148 Kiel, Germany

Corresponding author: Jacob Geersen (jgeersen@geomar.de)

Abstract

Tsunami earthquakes generate large tsunamis but only moderate ground shaking. The discrepancy between the magnitude of the surface wave and the resulting tsunami height makes them a serious threat to coastal communities and a problem for tsunami early warning. Although at least 13 tsunami earthquakes took place since 1896, there is little consent on what controls their genesis. It remains unclear if they are tied to distinct subduction-zone structures or geometries or if they can occur along all active margins. To help shed light on the genesis of these unusual earthquakes, I combine marine acoustic data from subduction-zone segments that experienced tsunami earthquakes in order to search for structural similarities in the nature of the subducting oceanic plate. The structural comparison indicates that tsunami earthquakes preferentially occur in regions where the subducting plate is characterized by excess topography which is not blanketed by trench sediment. While subducted, the topographic obstacles likely cause fracturing along their track. This contributes to the development of a thick, structurally and lithological complex, and fragmented plate-boundary shear-zone, which may be prone to fail at a low velocity during a tsunami earthquake. The results suggest that when assessing the risk of a tsunami earthquake, special focus should be placed on the combination of lower-plate topography and trench sediment thickness.

1. Introduction

Subduction related earthquakes are the main source for major tsunamis in the oceans. The moment magnitude (Mw.) 9.2 Aceh-Andaman (2004) and Mw. 9.1 Tohoku-Oki (2011) events are recent examples of giant tsunamigenic earthquakes that generated ocean-wide tsunamis (Titov et al., 2005; Fujii et al., 2011). Beside such large magnitude events, there is a second type of subduction thrust earthquakes capable of causing devastating tsunamis. These are tsunami earthquakes, which rupture near the trench and are characterized by long source durations and a reduced component of high-frequency energy (Kanamori et al., 1972; Satake and Tanioka, 1999; Okal and Newman, 2001; Bilek and Lay, 2002). Often, the tsunami is larger than expected given the small accompanying surface wave magnitude (Ms.) of the tsunami earthquake, and therefore catches coastal inhabitants by surprise, who have not or rarely felt the ground moving.

Since 1896, tsunami earthquakes occurred along the Sunda Arc (1907, 1994, 2006, 2010), in the Hikurangi subduction zone (March 1947, May 1947), off Peru (1960, 1996), along the Aleutian Islands (1946), off Nicaragua (1992), and along the Hokkaido - Kuril subduction zone (1896, 1963, 1975) (Fig. 1, Table 1). From the above listed earthquakes and associated tsunamis, only the New Zealand and Kuril events occurred without causing any known fatalities, either due to their remote locations (Kuril) or because the beaches were empty when the tsunamis arrived (New Zealand, McSaveney, 2006). In contrast, the 1896 Sanriku event off Hokkaido, the most tragic tsunami earthquake on the record, caused more than 27,000 fatalities and produced up-to 38 m high local tsunami run-ups (NGDC/WDC, 2018).

Tsunami earthquakes were initially described by Kanamori (1972) who noted the typical large discrepancy between tsunami height and surface wave magnitude. In 1992, the Nicaragua event was the first tsunami earthquake that was recorded by modern broadband seismometers (Kanamori and Kikuchi, 1993). In some cases the seismological observations have been related to certain subduction zone structures: For the 1947 New Zealand, 1992 Nicaragua, and 1994 Java events it has been discussed whether the unusual rupture characteristics might be caused by excess topography on the subducting plate (Abercrombie et al., 2001; Bilek and Lay, 2002; McIntosh et al., 2007; Bell et al., 2014). It has been suggested that in these three subduction-zones, subducting seamounts locally increase plate-coupling and therefore generate spatially limited asperities within the overall creeping (aseismic) section of the shallow plate-boundary (Tanioka et al., 1997; Abercrombie et al., 2001; Bilek and Lay, 2002). Other explanations for the genesis of tsunami earthquakes invoke propagation of the rupture within weak subducted sediments along the shallow plate-boundary (Kanamori, 1972; Pelayo and Wiens, 1992; Kanamori and Kikuchi, 1993; Satake and Tanioka, 1999; Polet and Kanamori, 2000), the activation of splay-faults in the marine forearc (von Huene et al., 2016; Fan et al., 2017) or inelastic shoving of unconsolidated sediments at the wedge toe under the action of shallow slip (Seno, 2000; Tanioka and Seno, 2001).

Tsunami earthquakes share many seismological characteristics, such as a long source duration, a reduced component of high-frequency energy, and rupture near the trench. Despite their seismological similarity, there is, however, no commonly accepted model for the structural or morphological conditions that are conducive to tsunami earthquakes. Bilek (2010) showed that tsunami earthquakes tend to occur at margins characterized as erosional, contrary to giant megathrust earthquakes that tend to rupture margins characterized as accretionary. This view was, however, challenged by the 2010 Mentawai and reevaluation of the 1907 offshore Sumatra tsunami earthquakes (Kanamori et al., 2010) as well as by the giant and tsunamigenic 2011 Tohoku-Oki earthquake. It is therefore not clear if tsunami earthquakes occur independently of the tectonic framework or if certain tectonic segments are more prone to tsunami earthquakes than others. Consequently, it is almost impossible to assess the risk which is associated to tsunami earthquakes for individual regions.

Here I combine published and unpublished multibeam bathymetric data from multiple cruises and different sources in order to characterize the structure of the subducting plate in all subduction-zone segments that experienced tsunami earthquakes since 1896. Where available the bathymetric information is complemented with published seismic reflection lines that image the character of the subducting plate prior to subduction and/or under the marine forearc. The picture that emerges from this study is that structurally and lithologically complex plate-boundaries that develop in regions of excess topography on the subducting-plate not leveled out by trench sediment preferentially accommodate tsunami earthquakes.

2. Materials and Methods

For each tsunami earthquake region I collated high resolution bathymetric data from German (http://www.bsh.de), French (http://en.data.ifremer.fr), Japanese (Japan Agency for Marine-Earth Science and Technology, 2016) and US (http://www.rvdata.us) research cruises as well as the compilation of data provided by the Global Multi-Resolution Topography (GMRT) synthesis (Ryan et al., 2009) (compare Tab. 1). The data from the individual research cruises were quality checked and manually edited if necessary. For the New Zealand margin, I further used the nationwide bathymetric compilation provided by The National Institute of Water and Atmospheric Research (NIWA) (Mitchell et al., 2012). The collated data is displayed on top of the SRTM15+ grid (Becker et al., 2009, Sandwell et al., 2014). The SRTM15+ grid interpolates ship-based bathymetric soundings with bathymetric predictions from gravity models at 15 arc-seconds spatial resolution. Bathymetric information from satellite gravity data does not provide as reliable depths as ship-based soundings. Therefore, and due to the different spatial resolution (coverage) of the different datasets, variations in lower-plate structure between the different study regions as well as within individual subduction-zone segments are only analyzed qualitatively. All collated bathymetric data (Fig. 2-8) have been uploaded as GeoTIFF files to the Pangaea data archive (https://doi.pangaea.de/10.1594/PANGAEA.899049). For each study

region, two versions are available: one that contains only shipborne data and a second where cells without shipborne data have been filled with SRTM15+ data.

In addition to the bathymetric maps, I further show the residual bathymetric data provided by Bassett and Watts (2015A, 2015B). In the residual grids, the long wavelength bathymetric gradient from the arc to the trench and the abyssal plain has been removed which helps to determine shorter wavelength bathymetric anomalies on the oceanic plate and in the marine forearc. For the latter, the short wavelength anomalies may reflect morphologic variations in the nature of the subducting plate. The bathymetric data are complemented with published seismic reflection profiles.

3. Results

3.1. Tsunami earthquakes off Hokkaido and the Kurils (1896, 1963, 1975)

The tsunami that was caused by the 1896 Sanriku earthquake (Fig. 2) devastated large parts of the adjacent coastlines with run-ups of up-to 38 m (NGDC/WDC, 2018). With more than 27,000 fatalities, this event represents the most tragic tsunami earthquake on record, and also the deadliest tsunami catastrophe in the history of Japan. While the surface wave magnitude of the 1896 earthquake was only 7.2, the large tsunami likely resulted from a slow rupture of the shallow plate-boundary close to the trench (Kanamori, 1972; Satake and Tanioka, 1999; Tanioka and Seno, 2001). Approximately 115 years later, the tsunamigenic Mw. 9.1 Tohoku-Oki earthquake ruptured the adjacent margin segment (Fig. 2), causing a comparable tsunami (in terms of regional run-up heights) despite much larger magnitude.

The 1963 Kuril tsunami earthquake occurred on 20 October 1963 (Fig. 2), seven days after the Mw. 8.5 Kuril Earthquake on 13 October 1963 (Fukao, 1979; Pelayo and Wiens, 1992). Although its moment magnitude (Mw. 7.8) was much lower compared to the main shock (Mw. 8.5), the resulting tsunami reached similar run-up heights of up-to 15 m (NGDC/WDC, 2018). The tsunami earthquake ruptured the shallow plate-boundary up-dip of the rupture area of the main shock. Approximately 12 years later, a comparable tsunami earthquake occurred ~300 km to the SW of the 1963 event. The 10 June 1975 event (Mw. 7.5) ruptured the shallow plate-boundary up-dip of a series of larger events including the eastern Hokkaido earthquake of 11 August 1969 and the Nemuro-Oki earthquake of 17 June 1973 (Fukao, 1979; Pelayo and Wiens, 1992).

Lower Plate Structure

The convergent margin between the 1896 and 1963 tsunami earthquakes accommodates subduction of the Early Cretaceous Pacific Plate under the Okhotsk Plate. Convergence occurs at

~9 cm/a towards the NW. Trench sediment thickness is generally low along the Hokkaido – Kuril Trench with less than 500 m in the area of the 1896 earthquake and less than 800 m in the area of the 1975 event (Kläschen et al., 1994; Kodaira et al., 2017). The oceanic plate seaward of the 1896 earthquake is dissected by multiple trench-parallel horst-and-graben structures which result from bending related normal faulting of the downgoing lithosphere. The vertical seafloor offset generated by the bend-faults ranges from around 100 m at 100 km seaward from the trench to 800 m near the deformation front (Fig. 2C; also compare Tsuru et al., 2000; Kodaira et al., 2017). 50 km landward from the trench, up-to 2000 m of vertical offset in the subducting oceanic basement have been observed in seismic reflection lines (Tsuru et al., 2000). The horst-and-grabens can be traced to the deformation front and are not blanketed by sediment, highlighting the sediment starved nature of the trench. The rupture area of the 1896 earthquake is located in an area of high residual bathymetry (up-to 1500 m) in the marine forearc which does not correspond to positive topography on the oceanic plate seaward of the trench. Because 2D seismic reflection lines do not provide evidence for anomalously large isolated subducting topography in the area (Tsuru et al., 2000; Kodaira et al., 2017) the genetic origin for the high residual bathymetry remains unknown.

Shipborne bathymetric coverage in the areas of the 1963 and 1975 earthquakes is sparse. Figure 2 shows multiple isolated seamounts located seaward of the trench near both rupture areas. A 2D seismic reflection line located close to the 1975 epicenter shows a comparable positive topography (10 km wide, 1.5 km high) in the subducting oceanic plate which may correspond to a subducting seamount (Fig. 2D). The 1975 epicenter is further located above two subducting fracture-zones (Wessel et al., 2015) but the seafloor expression of the fracture-zones is not well resolved due to the limited coverage with high resolution data. Bending related horst-and-grabens are present offshore both rupture areas, but absolute vertical fault offsets at the seafloor are only half the size (~150 m) compared to the area of the 1896 earthquake (Fujie et al., 2018).

3.2. Tsunami earthquakes off Sumatra (1907, 2010)

The 1907 Sumatra earthquake was originally located seaward of the trench in the outer rise of the Australian Plate (Gutenberg and Richter, 1954). Only after a thorough review of historical seismograms and comparison to recent Sumatran earthquakes, Kanamori et al. (2010) concluded that the event likely took place as a thrust event at the plate-boundary under the marine forearc (Fig. 3). They located the event to the SW of Simeulue Island with a location uncertainty of at least +/-1°. Despite its moderate magnitude (Mw. 7.8) the event caused a tsunami that affected ~1000 km of the Sumatran coast with >10 m high waves at Simeulue Island (Newcomb and McCann, 1987; McAdoo et al., 2006; Monecke et al., 2008).

The 25 October 2010 Mentawai earthquake (Fig. 3) represents the most recent tsunami earthquake. It ruptured the shallow plate-boundary seaward of the Pagai Islands with most slip

confined to depths shallower than 6 km (Hill et al., 2012). The rupture area extends >100 km along the margin and rupture lasted for ~90 s (Lay et al., 2011). The 2010 earthquake was located updip of the rupture area of a Mw. 8.4 earthquake that took place on 12 September 2007 (Collings et al., 2012; Hill et al., 2012).

Lower Plate Structure

Along the convergent margin of Sumatra, Eocene (1907 earthquake) to Late Cretaceous (2010 earthquake) oceanic lithosphere of the Australian Plate subducts under the Sunda Plate. Convergence occurs towards the NNE at rates between 5.4–5.9 cm/a. The thickness of the sedimentary trench-fill decreases southwards along the margin from 2000-2500 m in the area of the 1907 earthquake to around 1100 m seaward of the 2010 earthquake (Singh et al., 2011; Geersen et al., 2013). The Australian Plate is dissected by multiple N-S trending oceanic fracture-zones (Kopp et al., 2008; Jacob et al., 2014). From these, the 97° fracture-zone and the Investigator fracture-zone form distinct topographic highs at the seafloor (Fig. 3B). The 96° fracture-zone, which subducts in the region of the 1907 earthquake, is covered by trench sediment near the deformation front. In the marine forearc, the subducting part of the 96° fracture-zone corresponds to a residual bathymetric high with a similar trend (Fig. 3B). The estimated epicenter of the 1907 earthquake is located close to the subducting 96° fracture-zone and the bathymetric high in the marine forearc. Due to its +/- 1° location uncertainty (Kanamori et al., 2010), it is however, not possible to ultimately correlate the 1907 earthquake with structural features on the subducting plate.

The rupture area of the 2010 earthquake coincides with a section of the oceanic plate that is overprinted by multiple individual large seamounts seaward of the deformation front (Fig. 3A). The seamounts rise 600 – 3500 m from the surrounding seafloor. Two of the seamounts are located close to the deformation front at the northwestern and southeastern end of the rupture area of the 2010 earthquake. The fact that the two seamounts rise from the trench floor, indicates that the thickness of the trench sediment is too small to level out the rough topography of the oceanic plate. Bending related horst-and-grabens induce vertical seafloor offsets of up-to 200 m. The nearest published seismic reflection profile (CGGV020; Singh et al., 2011) is located to the southeast of the rupture area (Fig. 3A). The seismic line shows that the rough and morphologically complex oceanic basement is continuous into the subduction-zone (Fig. 3C).

3.3. Tsunami earthquake off the Aleutians (1946)

The Aleutian earthquake of 1 April 1946 (Mw. 8.2) ruptured a ~100 km long stretch (Fig. 4) of the Unimak segment of the Aleutian – Alaska margin (Johnson and Satake, 1997; Okal et al., 2002; von Huene et al., 2012; Miller et al., 2014). The tsunami that was produced by the

earthquake was observed in the entire Pacific Ocean and even in Antarctica (Okal et al., 2002). A local tsunami run-up of up-to 42 m at Scotch Cap Lighthouse on Unimak Island possibly resulted from a submarine slide triggered by the earthquake (von Huene et al., 2014). However, the far-field tsunami that reached heights of 17 m at Hawaii (NGDC/WDC, 2018) likely resulted from a slow rupture extending to the shallow plate-boundary (Johnson and Satake, 1997; Satake and Tanioka, 1999) and possibly along upper-plate splay-faults (von Huene et al., 2016).

Lower Plate Structure

In the region of the 1946 Aleutian tsunami earthquake, Paleoce to Eocene oceanic crust of the Pacific Plate subducts under the North American Plate. Subduction occurs towards the NW at a convergence rate of 6.7 cm/a (Fig. 4). Regional seismic lines show a maximum sediment thickness on the oceanic plate of around 1000 m adjacent to the deformation front (Fig. 4C) (von Huene et al., 2012, 2016). Bending-related faulting of the subducting plate is manifest by up-to 250 m high trench-parallel horst-and-grabens at the seafloor. In addition to bending related fault-scarps, the oceanic plate seaward of the rupture area of the 1946 earthquake caries multiple individual seamounts (Fig. 4). Most seamounts elevate between 500–1500 m from the surrounding seafloor. Seismic reflection data in the area of the 1946 earthquake are limited to a couple of lines with only one of them (Ewing line 1237) imaging the subducting oceanic basement to depth below the middle and upper continental slope (Fig. 4C) (also compare von Huene et al., 2012, 2016; Miller et al., 2014). The seismic line crosses two subducting seamounts which are located below the continental slope (pink circles in Fig. 4A) (von Huene et al., 2016). The subducting seamounts elevate 1000 – 1500 m from the subducting oceanic basement. Seismic line S.P.Lee-207 images another subducting seamount near the deformation front but does not resolve the subducting oceanic basement farther down-dip (Miller et al., 2014).

3.4. Tsunami earthquakes off New Zealand (1947)

The 25 March 1947 Poverty Bay (Mw. 7.0-7.1) and 17 May 1947 Tokomaru Bay (Mw. 6.9-7.1) earthquakes ruptured the northern Hikurangi margin (Fig. 5) in the area off the city of Gisborne (Doser and Webb, 2003; Bell et al., 2014). Both events share many characteristics of tsunami earthquakes, including long rupture durations and slow rupture speeds (Doser and Webb, 2003; Bell et al., 2014). The earthquakes occurred 10-15 km landward of the deformation front and rupture migrated updip to the shallow plate-boundary (Bell et al., 2014). The resulting tsunamis reached run-up heights of 6 m (Tokomaru Bay earthquake) and 10 m (Poverty Bay earthquake) which was much higher as expected from the earthquakes magnitudes (McSaveney, 2006; Bell et al., 2014; NGDC/WDC, 2018). Through calculating different rupture models for the Poverty Bay event and comparing them to the structural character of the subducting plate, Bell et al. (2014) suggested that slip evolved over a subducting seamount.

Lower Plate Structure

The subducting Pacific Plate in the area of the 1947 earthquakes is of Cretaceous age and convergence occurs at an angle of 260° and a velocity of 4.4 cm/a. Trench sediment thickness at the deformation front ranges around 1100 m (Barker et al., 2018). The oceanic plate seaward of the deformation front is overprinted by multiple large seamounts including the Tūranganui Knolls and Puke Knoll which are well recognizable in the residual bathymetric map (Fig. 5B). These seamounts elevate up-to 1500 m from the surrounding seafloor. A regional grid of seismic reflection and magnetic data indicates that multiple seamounts have already been subducted and are now located under the marine forearc (pink ellipses in Fig. 5; Barnes et al., 2010; Pedley et al., 2010, Bell et al., 2014; Barker et al., 2018). In the area of the 1947 earthquakes, the ellipses labeled S1 and S2 (Fig. 5A) represent subducted seamounts (Bell et al., 2014).

3.5. Tsunami earthquakes off Peru (1960, 1996)

The 20 November 1960 Peru tsunami earthquake (Fig. 6) occurred along a section of the South American Subduction zone that had experienced little seismicity and no large earthquakes in historic times (Nishenko, 1991). While the depth of the hypocenter is not well determined, there is good evidence that slip evolved along a shallow dipping (6°) thrust fault (Pelayo and Wiens, 1992). The earthquake generated tsunami reached run-up heights of up-to 9 m along the Peruvian coast and was also observed on the other side of the Pacific Ocean basin along the coast of Japan (Pelayo and Wiens, 1990; NGDC/WDC, 2018). The large tsunami likely resulted from slow rupture (130 s source duration) of the shallow plate-boundary as indicated by the modelled 6° dip of the fault plane (Pelayo and Wiens, 1990).

After the 1960 earthquake, the 21 February 1996 event (Fig. 6) was the second tsunami earthquake that occurred off Peru in the last century (Ihmlé et al., 1998; Satake and Tanioka, 1999). The epicenter was located ~335 km to the southeast of the 1960 event. Seismic rupture migrated updip from the epicenter over an along margin distance of ~100 km (Ihmlé et al., 1998). The combination of a low rupture velocity and rupture of the shallow plate-boundary produced local tsunami run up heights of 5 m (Ihmlé et al., 1998; Bourgeois et al., 1999; NGDC/WDC, 2018).

Lower Plate Structure

Along the section of the Peruvian margin where the tsunami earthquakes took place, Oligocene oceanic crust of the Nazca Plate subducts under the South American Plate. Convergence occurs towards an angle of ~80° at rates of 6.7-6.9 cm/a. Trench sediment thickness in the area of the 1960 earthquake ranges from ~300-700 m (Prince and Kulm, 1975; Bourgois et al., 1988). Farther south, in the area of the 1996 earthquake, the overall sediment thickness remains too

small (<500 m) to level out the topographic signature of the Mendana fracture-zone which can be recognized as topographic features all the way to the deformation front (Fig. 6; also compare Fig. 4 in Huchon and Bourgois, 1990).

At the latitude of the 1960 earthquake, two smaller seamounts rise up-to 400 m from the sedimentary trench-fill. The seamounts are intersected by trench parallel horst-and-grabens which are the surface expression of bending related faults. Bend faulting of the oceanic plate generates vertical seafloor displacements up-to 150 m. Around 7.5°S, the trench is intersected by the 10-20° trending Trujillo Trough (for a detailed discussion of the nature and origin of Trujillo Trough see Pautot and Bourgois (1986); Prince and Kulm, 1975; Huchon and Bourgois, 1990). The subducted part of Trujillo Trough, extrapolated into the subduction zone, correlates with the region of the 1960 epicenter (Fig. 6A). On its southeastern side, Trujillo Trough is bound by a left-lateral transpressive fault (Huchon and Bourgois, 1990). Shortening across the fault has led to the formation of the up-to 1000 m high southeastern escarpment which is well expressed in seismic (Fig. 6C; Prince and Kulm, 1975; Huchon and Bourgois, 1990) and the residual bathymetric (Fig. 6B, Huchon and Bourgois, 1990) data.

The rupture area of the 1996 earthquake coincides with the location of the subducting Mendana Fracture Zone (Fig. 6A). Bathymetric data collected during RV Jean Charcot SEAPERC cruise in 1986 (Pautot and Bourgois, 1986; Bourgois et al., 1988), image the fracture zone as a series of parallel ridges with elevations of up-to 1000 m compared to the surrounding seafloor (Fig. 6A; Huchon and Bourgois, 1990). Single-channel seismic line 120, which was collected during the same cruise, shows that the ridges are isolated features with little sediment cover in-between (Fig. 6D). The Mendana Fracture Zone is subducted along with the Nazca Plate into the area that ruptured during the 1996 earthquake. In the marine forearc, the residual bathymetry shows a positive anomaly at the middle slope which coincides with the subducting fracture-zone (Fig. 6B).

3.6. Tsunami earthquake off Nicaragua (1992)

The 2 September 1992 Nicaragua earthquake ruptured the shallow plate-boundary for 250 km along-strike (Fig. 7A; Satake, 1994). The largest moment release occurred within two regions which are located within the northwestern and southeastern edges of the rupture area (red dashed ellipses in Fig. 7A) (Ihmlé, 1996). Shallow thrust faulting in combination with a long source duration of ~100 s (Satake and Tanioka, 1999) resulted in up-to 10 m high tsunami run-ups in Nicaragua (Satake, 1994; NGDC/WDC, 2018).

Lower Plate Structure

Off Nicaragua, the Oligocene oceanic Cocos Plate subducts under the Caribbean Plate towards 22°E and with a convergence velocity of 7.4 cm/a. Trench sediment thickness on the oceanic plate remains thin along the entire margin and usually ranges between 300-400 m (McIntosh et al., 2007). Bending of the oceanic plate is expressed in trench-parallel fault scarps with vertical seafloor displacements of up-to 400 m. Seaward of the deformation front, multiple individual seamounts rise from the surrounding oceanic basement (Fig. 7A). The seamounts, which are easily recognized in multibeam bathymetric data, have diameters between 5000-15000 m and heights of up-to 1300 m. Based on a regional grid of 2D seismic reflection lines (e.g. Fig. 7C), subducting seamounts have also been imaged under the marine forearc (pink circles in Fig. 7A; McIntosh et al., 2007; Sallares et al., 2013). The subducted seamounts are located within the regions of high moment release of the 1992 earthquake as identified by Ihmlé (1996). In the marine forearc, the subduction of the seamounts on the Cocos Plate has led to local over-steepening of the continental slope and subsequent gravitational collapse, which is manifested in the wide occurrence of submarine slope failures (white polygons in Fig. 7A; Harders et al., 2011).

3.7. Tsunami earthquakes off Java (1994, 2006)

Prior to 1994, no large thrust earthquake had been instrumentally recorded along the Java margin leading to the assumption of a weakly coupled subduction-zone (Scholz and Campos, 2012). With a source duration of 80-95 s (Abercrombie et al., 2001; Bilek and Engdahl, 2007) the 1994 Java earthquake was slightly faster than other tsunami events such as the 1992 Nicaragua earthquake. While the epicenter was located near the trench, highest slip has been modeled farther landward under the outer-arc high (Fig. 8, Abercrombie et al., 2001; Bilek and Engdahl; 2007). A special characteristic of the 1994 event was the predominance of normal faulting aftershocks (Polet and Kanamori, 2000). Based on the slip distribution, the dominance of normal faulting aftershocks, and local tsunami arrival times, Abercrombie et al. (2001) suggested that the 1994 event ruptured the plate-boundary in the area of a subducted seamount.

With more than 800 fatalities, the 2006 Java earthquake was the deadliest tsunami earthquake since the beginning of the 20th century (NGDC/WDC, 2018). The event is located ~600 km to the west of the 1994 event (Fig. 8A) and had local tsunami run-up heights of 21 m (NGDC/WDC, 2018). A long source duration of 185 s, rupture near the trench, and the larger than expected tsunami (Ms. 7.2) classify the 2006 event as a tsunami earthquake (Ammon et al., 2006). It has been speculated that the 2006 earthquake may have been laterally bounded by excess topography on the subducting plate (Bilek and Engdahl, 2007; Bassett and Watts, 2015A) but the lack of high-resolution marine geophysical data in the area complicates the analyses. Furthermore, Fan et al. (2017) showed evidence that upper-plate faults may have been involved in the second stage of the rupture therewith contributing to the tsunami.

Lower Plate Structure

Off Java, Cretaceous oceanic basement of the Australian Plate subducts under the Sunda Plate. Convergence occurs around an angle of 14° and a velocity of 7.0 cm/a. While Lüschen et al. (2011) report a maximum trench sediment thickness of 1000 m for the larger area the trench sediments in the area of the 1994 earthquake likely do not exceed a few hundreds of meters. The thickness of the sedimentary trench-fill seaward of the 2006 rupture area cannot ultimately be resolved due to the lack of seismic reflection data, but possibly ranges somewhere between 1300 m as observed farther to the west and the almost sediment starved trench to the east (1994 earthquake area) (Kopp et al., 2006). It has been noted by several authors that Java represents an endmember margin in terms of lower-plate roughness and complexity (e.g. Kopp et al., 2006).

In the region of the 1994 earthquake, trench parallel horst-and-grabens show vertical seafloor offsets up-to 300 m (Fig. 8A). The oceanic plate seaward of the deformation front is characterized by multiple topographic highs which rest on an overall thickened section of oceanic crust. The thickened crust and its complex structure in the area of the 1994 earthquake corresponds to the Roo Rise, which represents a residual bathymetric anomaly with amplitude > 2000 m (Fig. 8B; Kopp et al., 2006; Shulgin et al., 2011; Bassett and Watts, 2015A). Based on seismic reflection and refraction data, Shulgin et al. (2011) and Lüschen et al. (2011) showed that the rough and elevated structure of the Roo Rise continuous into the subduction-zone (Fig. 8D) which is further expressed by shallowing of the seafloor of ~1000 m (Kopp et al., 2006) and high residual bathymetry in the area of the lower and middle continental slope (Bassett and Watts, 2015A, 2015B). This has been attributed to uplift and deformation of the upper-plate above the subducting Roo Rise. The complex structure of the Roo Rise and the bend-fault scarps can be traced to the deformation front without being leveled out by a sedimentary trench-fill.

Multibeam bathymetric data imaging the oceanic plate and the marine forearc in the area of the 2006 earthquake is sparse and limited to the adjacent margin segments to the west (Kopp and Kukowski, 2003) and east (Kopp et al., 2006). Seaward of the deformation front, the oceanic plate is overprinted by trench perpendicular ridges that elevate up-to 800 m from the surrounding seafloor (Fig. 8C). Striking parallel to the magnetic anomalies of the oceanic basement, the ridges likely represent seafloor spreading fabric. Large seamounts rising up-to 4000 m above the seafloor as well as multiple smaller seamounts (1000 m high) are located on the oceanic plate seaward of the rupture area. The largest seamount corresponds to the Christmas Island. Residual bathymetry in the 2006 rupture area is generally low (compared to the 1994 rupture area) but isolated anomalies of ~1000 m are present at multiple locations (Fig. 8B). Considering the high density of seamounts on the oceanic plate seaward of the deformation front, these isolated anomalies may correspond to subducting seamounts. A high residual anomaly to the east of the 2006 rupture area has been interpreted as a large subducting seamount which may have stopped eastward propagation of the earthquake (Bilek and Engdahl, 2007).

4. Discussion

In the following I compare the structure and morphology of the subducting plates in all tsunami earthquake areas and discuss how the shared structural characteristics may relate to the phenomenon of tsunami earthquakes. Subsequently, I discuss the occurrence of tsunami earthquakes and the parameters that might govern their spatial distribution in relation to large tsunamigenic megathrust events.

4.1. Lower-plate structural characteristics in tsunami earthquake regions

From the structural comparison of 13 tsunami earthquake zones, I do not find any striking similarities in the large-scale plate-tectonic configurations. The age of the subducting basement ranges from Oligocene (Nicaragua, Peru) to Early Cretaceous (Hikurangi, Java, Hokkaido, Kuril) and the convergence rate ranges from 4.4 cm/a (Hikurangi) to 9.2 cm/a (Hokkaido). The obliquity of plate-convergence (90° = orthogonal) is 50°-85° and thus does not show a systematic pattern, either (Tab. 2).

Notable similarities between the tsunami earthquake areas, however, include the thickness of the sedimentary trench-fill and the morphology of the subducting plate. 12 out of 13 tsunami earthquakes (with the exception of the 1907 Sumatra event) occurred in subduction-zone segments, in which the trench is starved or only partly filled with sediment (Tab. 2, Fig. 9). For these 12 events the maximum sediment thickness is 1100 m in the area of the 1947 New Zealand earthquakes. In other tsunami earthquake regions (e.g. 1996 Peru, 1994 Java) almost no sediment is located within the trench.

In addition to carrying little to no trench sediment, all subducting plates in tsunami earthquake regions host a rough and morphologically complex oceanic basement. In some segments the rough basement is present in the form of multiple large (up-to 3500 m) seamounts that elevate from the oceanic crust (1946 Aleutian, 1947 New Zealand, 1992 Nicaragua, 2010 Mentawai). In other regions the morphologically complex basement is present in the form of spatially continuous topographic features. These features include the ~100 km wide and up-to 1000 m high Mendena Fracture Zone (1996 Peru), the 2500 m high thickened section of oceanic crust corresponding to the Roo Rise (1994 Java), and the 1000 m high southeastern escarpment of the Trujillo Trough (1960 Peru). In the area of the 2006 Java earthquake, multibeam bathymetric data from the oceanic plate is limited to two margin parallel tracks. These profiles image multiple trench perpendicular ridges (Fig. 6B) that were likely generated during seafloor spreading. With elevations of up-to 800 m, the ridges likely exceed the regional trench-fill. In addition to the ridges, multiple (>20) seamounts in the larger area complete the picture of a rough and morphologically complex oceanic plate (Fig. 6A).

The above observations are mainly from subducting oceanic plates seaward of the trench, and hence before subduction. A critical question is whether the observed complex morphologies are representative for the already subducted part of the plates under the marine forearc? In areas where seismic reflection data is available (1946 Aleutian, 1947 New Zealand, 1992 Nicaragua, 1994 Java, 2010 Mentawai), similarly complex basement topography has been imaged beneath the marine forearc within the rupture areas of the tsunami earthquakes (Figs. 2,3,5,6,8). For many areas without seismic data coverage, the residual bathymetric anomalies indicate that many topographic features seaward of the trench continue into the subduction-zones (e.g. Java - Roo Rise; Fig. 8B). Furthermore, the continuation of morphologic features can be assumed based on their natural shapes or patterns of occurrences observed elsewhere. For spatially continuous morphologic features, such as Trujillo Trough (1960 Peru earthquake), Roo Rise (1994 Java earthquake), Mendena Fracture Zone (1996 Peru earthquake), and likely also the spreading related ridges off Java (2006 Java earthquake), there is little that argues against a continuation of these features into the subduction zone. In contrast, the presence of individual seamounts seaward of the deformation front cannot directly be extended into the subduction zone. However, global censuses show that seamounts taller than 1000 m tend to occur in clusters (Kim and Wessel, 2011). The vast majority of the seamounts observed seaward of the rupture areas of the 1946 Aleutian, 1947 New Zealand, 1992 Nicaragua, 2006 Java, and 2010 Mentawai earthquakes rise >1000 m from the surrounding seafloor. Moreover, the seafloor in all areas is largely overprinted by seamounts resulting in a high seamount density. Whether seamount density as well as the size of the individual seamounts remains identical for the subducted part of the plates (or if it increases or decreases) can, however, only be answered with a dense grid of seismic reflection lines. Considering these aspects, the morphologically complex oceanic basement seaward of all tsunami earthquake areas is most likely also present along the shallow plate-boundary.

The 1907 Sumatra tsunami earthquake represents an outlier from the list with respect to the thickness of the sediments in the adjacent trench, which exceeds 2000 m (Geersen et al., 2013). The exact location of the epicenter is not well determined, but even with an uncertainty of +/- 1°, the probability is high that the area that ruptured during the event includes the subducting part of the 96° fracture-zone (Fig. 3). Fracture-zones in the area usually form large (up-to 1500 m) positive topographic anomalies in the top of the oceanic basement (Geersen et al., 2015; Singh et al., 2017). Because the décollement offshore Northern and Central Sumatra forms deep within the trench-sediments (e.g. Cook et al., 2014) the plate-boundary in the area of the 1907 earthquake is likely altered by the subducting 96° fracture-zone.

Both, a rough and morphologically complex subducting oceanic basement as well as sediment starved and partially filled trenches are not unique to regions that experienced tsunami earthquakes. However, it is the combination of these two characteristics that seem to be important from the available record of tsunami earthquakes and therefore might be a crucial parameter in governing the distribution of such events.

4.2. How do sediment starved trenches and rough subducting plates promote tsunami earthquakes?

While the assumption that subducting lower-plate topography influences the style of seismicity has been proposed more than 40 years ago (Kelleher and McCann, 1976), the exact role of subducting topography for seismogenesis remains unclear (Cloos, 1992; Kodaira et al., 2000; Wang and Bilek, 2011, 2014; Saffer and Wallace, 2015; Scholl et al., 2015). The data presented here suggests that tsunami earthquakes preferentially occur in margin segments where little sediment is in the trench and where the oceanic plate is rough. Reconsidering different models on how subducting lower-plate topography may influence the structure and physical properties of the plate-boundary, there seem to be multiple explanations why sediment-starved trenches and rough subducting plates could be conducive to tsunami earthquakes:

1) Subducting lower-plate topography that sticks out from the subducting sediment section, is interpreted to alter the structural development of the plate-boundary (Fig. 10). In a conceptual model, Wang and Bilek (2011) suggested that a geometrically complex plate-boundary, composed of many individual small-scale faults, develops around and above a subducting seamount. This interpretation is supported by analogue (Dominguez et al., 1998, 2000) and numerical models (Ruh et al., 2016). If seismic rupture arrives at such a structurally and geometrically complex plate-boundary, it has to jump and propagate across multiple individual faults. This may slow down the rupture speed.

2) The subduction of a morphologically complex and rough oceanic plate promotes the development of a thick and lithological heterogeneous tectonic mélange (Fagereng and Sibson, 2010). The plate-boundary shear-zone may thus include marine sediments, the framework rock of the upper-plate and altered and unaltered basement rock from the oceanic plate (Fig. 10). In such a mixture of lithologies and grain-sizes, ductile deformation usually competes with brittle failure (Saffer and Wallace, 2015; Bürgmann, 2018). This diminishes the effectiveness of seismic rupture and likely reduces rupture velocity during an earthquake (Fagereng and Sibson, 2010; Saffer and Wallace, 2015; Festa et al., 2018).

3) Excess topography on the lower-plate modifies the amount of surrounding sediment. Seismic profiles across the Mendana Fracture Zone (1996 Peru tsunami earthquake region) show that the fracture-zone related troughs carry an additional sediment load (Fig. 6d). If the troughs stay intact during subduction, the contained sediments may provide sufficient fluid to locally increase fluid-pressure at the shallow plate-boundary. For the Hikurangi margin (1947 Poverty Bay and Tokomaru Bay tsunami earthquakes), Bell et al. (2010) and Barker et al. (2018) showed that seamount subduction causes the décollement to step up-to the crest of the seamount enabling anomalously thick lenses of fluid-rich sediment to be subducted around it. However, excess topography on the oceanic plate may also reduce the thickness of the surrounding sediment section by reducing the accommodation space. Such changes in subducting sediment thickness therefore likely redistribute fluid-pressure at the shallow plate-boundary (Fig. 10). This may

locally induce highly over-pressured patches along the plate-boundary shear-zone. Sedimentary induced changes in fluid-pressure in combination with the low rigidity of the sediments along the shallow plate-boundary (prior to any significant compaction and dehydration), therefore likely contribute to the reduced rupture speed of a tsunami earthquake (Ruff, 1989; Pelayo and Wiens, 1992; Kanamori and Kikuchi, 1993; Satake and Tanioka, 1999; Polet and Kanamori, 2000).

Following the discussion above, I consider it as likely that a tsunami earthquake results from the combined effect of a thick, structurally and lithological complex, and fragmented plate-boundary around and above subducting lower-plate relief which is not covered by subducting sediment (Fig. 10). There is no threshold with respect to the height of a subducting feature necessary to cause a tsunami earthquake. However, the height of the feature needs to be larger than the thickness of the underthrust sediment section (i.e. higher than the proto-décollement). Whether the actual décollement reacts to the height of the topographic feature, i.e. if it steps up-to the top of the feature (as discussed for the Hikurangi seamount; Bell et al., 2014; Barker et al., 2018) is another question. In some settings, sedimentary induced variations in fluid-pressure at the plate-boundary may further reduce rupture velocities. Whether fault rupture is fast enough to generate a tsunami earthquake, or if it occurs as slow slip event, may depend on the three dimensional distribution of fault geometry, roughness, lithology and fluid-pressure. The size of the anomalous plate-boundary may well exceed the size of the subducting topographic obstacle, especially in up-dip and down-dip direction (Dominguez et al., 1998, 2000; Ruh et al., 2016). During some tsunami earthquakes peak slip was concentrated within spatially limited patches of less than 50 km width (e.g. 1947 New Zealand, Bell et al., 2014; 1992 Nicaragua, Ihmlé, 1996). This suggests that large individual seamounts such as located offshore Hikurangi (Tūranganui Knolls, Fig. 5), Hokkaido (Erimo Seamount, Fig. 2), or the 2010 Mentawai rupture area (Fig. 3) may already alter a sufficient section of the plate-boundary to pre-condition a tsunami earthquake.

4.3. How do tsunami earthquakes interact with large tsunamigenic earthquakes?

From the 1964 Alaska (Mw. 9.2) until the 2010 Maule (Mw. 8.8) earthquake, no event of Mw. 8.8 or larger has ruptured a region that had been previously (or afterwards) failed in a tsunami earthquake (Fig. 9). In 2011, however, the 2011 Tohoku-Oki earthquake ruptured the area adjacent to the 1896 Sanriku tsunami earthquake (Figs. 2 and 9). Considering the uncertainties in the location and spatial extent of rupture areas for such historic events it is possible that the 2011 Tohoku-Oki earthquake re-ruptured the shallow plate-boundary in the area of the 1896 Sanriku event as already suggested by different authors (e.g. Yamazaki et al., 2018).

Interestingly, the shallow rupture of the 2011 Tohoku-Oki earthquake shared some characteristics of tsunami earthquakes including a reduced rupture speed and a reduced component of high-frequency energy (Koketsu et al., 2011; Lay and Kanamori, 2011). It has also been suggested that the 2004 Aceh-Andaman earthquake included a component of tsunami earthquakes (Seno and Hirata, 2007). In the case of the 2015 Illapel earthquake (Fig. 9; Central

Chile), a late tsunami stage was proposed by Lay et al. (2016) and Lee et al. (2016). Interestingly, the Illapel event occurred in a region of multiple well documented subducting seamounts in the South (Lange et al., 2016) and the Challenger fracture zone in the North (Poli et al., 2017). In particular the postulated late and slow southern and northern parts of the rupture (Lay et al., 2016; Lee et al., 2016) coincide with these subducting obstacles.

The above observations suggest that if a spatially limited patch of a plate-boundary, which fulfills the criteria to rupture as a tsunami earthquake, is located within the rupture area of a large or giant earthquake, a shallow tsunami-earthquake component may accompany failure of the deeper seismogenic zone. This scenario may account for tsunami earthquakes preconditioned by large individual subducting seamounts but maybe not for events related to spatially continuous topographic features such as basement ridges or fracture-zones.

The 1963 and 1975 Kuril and the 2010 Mentawai earthquakes occurred up-dip of the rupture area of great earthquakes. The series of the individual events indicates that great and likely giant earthquake ruptures that do not propagate to the trench (such as the 2007 event off Sumatra) may promote tsunami earthquakes farther up-dip (Collings et al., 2012; Hill et al., 2012).

4.4. Which other subduction-zones may host tsunami earthquakes?

To date, no tsunami earthquake has been reported as a repeater of a previous event (Fig. 9). This indicates a long (centenary to millennial) recurrence rate (if not occurring randomly). However, more than half of the world's deep-sea trenches are classified as sediment starved or partly sediment filled (Fig. 9; Geersen et al., 2018). With possibly more than 50,000 seamounts in the oceans (e.g. Kim and Wessel, 2011) the seafloor is littered with seamounts and other complex topographic features (e.g. fracture zones, basement ridges). As a consequence, many shallow subduction-zone segments located adjacent to sediment starved or partly sediment filled trenches host a rough oceanic basement that is not covered by subducting sediment. Despite the overall rare occurrence of tsunami earthquakes, one therefore has to consider the possibility that many shallow plate-boundaries may generate tsunami earthquakes.

This interpretation supports previous investigations of seismicity patterns in shallow subduction-zones. Different authors already noted a systematic occurrence of slow earthquakes within many shallow subduction-zones (e.g. Houston, 2001; Bilek and Lay, 2002; Bilek et al., 2004; Şen et al. 2015). This accounts for events which were recorded teleseismically (e.g. Bilek and Lay, 2002) as well as for events recorded by local networks (e.g. Şen et al., 2015). However, the global studies also show that earthquakes which rupture shallow plate-boundaries are not exclusively slow. Instead shallow plate-boundaries seem to host events with normal as well as unusually long source durations (e.g. Fig. 15.4 in Lay and Bilek, 2007). This study suggests that subducting topographic reliefs not leveled out by trench sediments contribute to reducing the rupture velocity of a shallow plate-boundary earthquake. Whether such an event ruptures a sufficient

area to cause a significant tsunami (i.e. to evolve into a tsunami earthquake) may depend, among other parameters, on the areal extent and three-dimensional distribution of the complex plate-boundary in association with subducting lower-plate relief.

5. Conclusions

Tsunami earthquakes which occurred since 1896 were largely bound to regions characterized by excess topography on the subducting plate which is not blanketed by trench and subducting sediment. The subducting topographic obstacles favor the development of a geometrically and structurally complex plate-boundary made of multiple individual faults with limited spatial extents. The long source duration that is characteristic for tsunami earthquakes is likely supported by the fact that within such a complex fault network, seismic rupture has to migrate and jump across multiple faults. The complex plate-boundary seems to be the most important factor that governs the occurrence of tsunami earthquakes, while increased plate-coupling around the subducting topographic features may enhance the amount of slip or reduce the earthquake recurrence rate. Future studies that help to increase the resolution of geophysical imaging of subducting lower-plate topography, in combination with better spatial and temporal resolution of small-scale seismicity, inter-seismic plate-coupling, and large earthquake ruptures will help to further untangle the role of subducting lower-plate relief for tsunami earthquakes. Considering the growing amount of shipborne bathymetric data it may be possible at some point to apply quantitative approaches for investigating the role of subducting-plate roughness in promoting tsunami earthquakes. At least when all margins which experienced tsunami earthquakes have been mapped to a similar extent with shipborne bathymetric data.

Acknowledgments

I thank Dirk Kläschen for help with collating the seismic images and Ingo Klaucke for help with handling of the SEAPERC bathymetric data. Satish Singh, Shuichi Kodaira, Alexey Shulgin and Dan Barker kindly provided seismic images from their publications. Heidrun Kopp, Jan Behrmann, Dietrich Lange, and Ingo Grevemeyer are thanked for discussion.

Access to Data

Access to field data:

The bathymetric data from German research vessels (R/V SONNE, R/V METEOR) can be requested through the German Bundesamt für Seeschifffahrt und Hydrographie (BSH) (http://www.bsh.de). Bathymetric data collected during US cruises (R/V Roger Revelle, R/V Maurice Ewing) are available from the Rolling Deck to Repository (R2R) web site (http://www.rvdata.us/). The SISMER (Systèmes d'informations scientifiques de la Mer) portal which is maintained by IFREMER regulates access to the bathymetric data from the SEAPERC

cruise of the French R/V Jean Charcot (http://en.data.ifremer.fr/SISMER). Access to the bathymetric data from the Hikurangi margin is possible through NIWA marine data repository (https://marinedata.niwa.co.nz/project-map-sam/). Data from the Japanese research vessel R/V KAIREI can be requested through the Data and Sample Research System for Whole Cruise Information (DARWIN) maintained by the Japan Agency for Marine-Earth Sciences (JAMSTEC).

Access to processed data:

The collated bathymetric data shown in Figures 2-8 can be downloaded as GeoTIFF files from the PANGAEA data archive (https://doi.pangaea.de/10.1594/PANGAEA.899049). The data are available with and without SRTM15+ filling in the background.

References

Abercrombie, R. E., Antolik, M., Felzer, K., & Ekström, G. (2001). The 1994 Java tsunami earthquake: Slip over a subducting seamount. Journal of Geophysical Research: Solid Earth, 106(B4), 6595–6607.

Ammon, C. J., Kanamori, H., Lay, T., & Velasco, A. A. (2006). The 17 July 2006 Java tsunami earthquake. Geophysical Research Letters, 33(24), L24308.

Barker, D. H., Henrys, S., Caratori Tontini, F., Barnes, P. M., Bassett, D., Todd, E., & Wallace, L. (2018). Geophysical Constraints on the Relationship Between Seamount Subduction, Slow Slip, and Tremor at the North Hikurangi Subduction Zone, New Zealand. Geophysical Research Letters, 45(23), 12-804.

Barnes, P. M., Lamarche, G., Bialas, J., Henrys, S., Pecher, I., Netzeband, G. L., … Crutchley, G. (2010). Tectonic and geological framework for gas hydrates and cold seeps on the Hikurangi subduction margin, New Zealand. Marine Geology, 272(1–4), 26–48.

Bassett, D., & Watts, A. B. (2015A). Gravity anomalies, crustal structure, and seismicity at subduction zones: 1. Seafloor roughness and subducting relief. Geochemistry, Geophysics, Geosystems, 16(5), 1508-1540.

Bassett, D., & Watts, A. B. (2015B). Gravity anomalies, crustal structure, and seismicity at subduction zones: 2. Interrelationships between fore-arc structure and seismogenic behavior. Geochemistry, Geophysics, Geosystems, 16(5), 1541-1576.

Becker, J. J., Sandwell, D. T., Smith, W. H. F., Braud, J., Binder, B., Depner, J., … Weatherall, P. (2009). Global Bathymetry and Elevation Data at 30 Arc Seconds Resolution: SRTM30_PLUS. Marine Geodesy, 32(4), 355–371.

Bell, R., Sutherland, R., Barker, D. H., Henrys, S., Bannister, S., Wallace, L., & Beavan, J. (2010). Seismic reflection character of the Hikurangi subduction interface, New Zealand, in

the region of repeated Gisborne slow slip events. Geophysical Journal International, 180(1), 34-48.

Bell, R., Holden, C., Power, W., Wang, X., & Downes, G. (2014). Hikurangi margin tsunami earthquake generated by slow seismic rupture over a subducted seamount. Earth and Planetary Science Letters, 397, 1–9.

Bilek, S. L., & Lay, T. (2002). Tsunami earthquakes possibly widespread manifestations of frictional conditional stability. Geophysical Research Letters, 29(14), 18–1.

Bilek, S. L., Lay, T., & Ruff, L. J. (2004). Radiated seismic energy and earthquake source duration variations from teleseismic source time functions for shallow subduction zone thrust earthquakes. Journal of Geophysical Research: Solid Earth, 109(B9).

Bilek, S. L., & Engdahl, E. R. (2007). Rupture characterization and aftershock relocations for the 1994 and 2006 tsunami earthquakes in the Java subduction zone. Geophysical Research Letters, 34(20), L20311.

Bilek, S. L. (2010). The role of subduction erosion on seismicity. Geology, 38(5), 479–480.

Bourgeois, J., Petroff, C., Yeh, H., Titov, V., Synolakis, C. E., Benson, B., … Norabuena, E. (1999). Geologic Setting, Field Survey and Modeling of the Chimbote, Northern Peru, Tsunami of 21 February 1996. Pure and Applied Geophysics, 154(3), 513–540.

Bourgois, J., Pautot, G., Bandy, W., Boinet, T., Chotin, P., Huchon, P., … von Huene, R. (1988). Seabeam and seismic reflection imaging of the tectonic regime of the Andean continental margin off Peru (4°S to 10°S). Earth and Planetary Science Letters, 87(1), 111–126.

Bürgmann, R. (2018). The geophysics, geology and mechanics of slow fault slip. Earth and Planetary Science Letters, 495, 112-134.

Cloos, M. (1992). Thrust-type subduction-zone earthquakes and seamount asperities: A physical model for seismic rupture. Geology, 20(7), 601–604.

Collings, R., Lange, D., Rietbrock, A., Tilmann, F., Natawidjaja, D., Suwargadi, B., ... & Saul, J. (2012). Structure and seismogenic properties of the Mentawai segment of the Sumatra subduction zone revealed by local earthquake traveltime tomography. Journal of Geophysical Research: Solid Earth, 117(B1).

Cook, B. J., Henstock, T. J., McNeill, L. C., & Bull, J. M. (2014). Controls on spatial and temporal evolution of prism faulting and relationships to plate boundary slip offshore north-central Sumatra. Journal of Geophysical Research: Solid Earth, 119(7), 5594-5612.

DeMets, C., Gordon, R. G., & Argus, D. F. (2010). Geologically current plate motions. Geophysical Journal International, 181(1), 1–80.

Dominguez, S., Lallemand, S. E., Malavieille, J., & von Huene, R. (1998). Upper plate deformation associated with seamount subduction. Tectonophysics, 293(3–4), 207–224.

Dominguez, S., Malavieille, J., & Lallemand, S. E. (2000). Deformation of accretionary wedges in response to seamount subduction: Insights from sandbox experiments. Tectonics, 19(1), 182–196.

Doser, D. I., & Webb, T. H. (2003). Source parameters of large historical (1917–1961) earthquakes, North Island, New Zealand. Geophysical Journal International, 152(3), 795–832.

Fagereng, Å., & Sibson, R. H. (2010). Melange rheology and seismic style. Geology, 38(8), 751-754.

Fan, W., Bassett, D., Jiang, J., Shearer, P. M., & Ji, C. (2017). Rupture evolution of the 2006 Java tsunami earthquake and the possible role of splay faults. Tectonophysics, 721, 143–150.

Festa, A., Dilek, Y., Mittempergher, S., Ogata, K., Pini, G. A., & Remitti, F. (2018). Does subduction of mass transport deposits (MTDs) control seismic behavior of shallow–level megathrusts at convergent margins?. Gondwana Research, 60, 186-193.

Fujii, Y., Satake, K., Sakai, S., Shinohara, M., & Kanazawa, T. (2011). Tsunami source of the 2011 off the Pacific coast of Tohoku Earthquake. Earth, Planets and Space, 63(7), 815–820.

Fujie, G., Kodaira, S., Kaiho, Y., Yamamoto, Y., Takahashi, T., Miura, S., & Yamada, T. (2018). Controlling factor of incoming plate hydration at the north-western Pacific margin. Nature communications, 9(1), 3844.

Fukao, Y. (1979). Tsunami earthquakes and subduction processes near deep-sea trenches. Journal of Geophysical Research: Solid Earth, 84(B5), 2303-2314.

Geersen, J., McNeill, L., Henstock, T. J., & Gaedicke, C. (2013). The 2004 Aceh-Andaman Earthquake: Early clay dehydration controls shallow seismic rupture. Geochemistry, Geophysics, Geosystems, 14(9), 3315–3323.

Geersen, J., Bull, J. M., McNeill, L. C., Henstock, T. J., Gaedicke, C., Chamot-Rooke, N., & Delescluse, M. (2015). Pervasive deformation of an oceanic plate and relationship to large> Mw 8 intraplate earthquakes: The northern Wharton Basin, Indian Ocean. Geology, 43(4), 359-362.

Geersen, J., Voelker, D., & Behrmann, J. H. (2018). Oceanic Trenches. In Submarine Geomorphology, 409-424. Springer, Cham.

Gutenberg, B., & Richter, C. F. (1954). Seismicity of the Earth and Associated Phenomena, 2nd edn, p. 310, Princeton Univ. Press, Princeton.

Harders, R., Ranero, C. R., Weinrebe, W., & Behrmann, J. H. (2011). Submarine slope failures along the convergent continental margin of the Middle America Trench. Geochemistry, Geophysics, Geosystems, 12(6), Q05S32.

Hill, E. M., Borrero, J. C., Huang, Z., Qiu, Q., Banerjee, P., Natawidjaja, D. H., … Sieh, K. (2012). The 2010 Mw 7.8 Mentawai earthquake: Very shallow source of a rare tsunami

earthquake determined from tsunami field survey and near-field GPS data. J. Geophys. Res., 117(B6), B06402.

Huchon, P., & Bourgois, J. (1990). Subduction-induced fragmentation of the Nazca Plate off Peru: Mendana Fracture Zone and Trujillo Trough revisited. Journal of Geophysical Research: Solid Earth, 95(B6), 8419–8436.

von Huene, R., Miller, J. J., & Weinrebe, W. (2012). Subducting plate geology in three great earthquake ruptures of the western Alaska margin, Kodiak to Unimak. Geosphere, 8(3), 628–644.

von Huene, R., Kirby, S., Miller, J., & Dartnell, P. (2014). The destructive 1946 Unimak near-field tsunami: New evidence for a submarine slide source from reprocessed marine geophysical data. Geophysical Research Letters, 41(19), 2014GL061759.

von Huene, R., Miller, J. J., Klaeschen, D., & Dartnell, P. (2016). A Possible Source Mechanism of the 1946 Unimak Alaska Far-Field Tsunami: Uplift of the Mid-Slope Terrace Above a Splay Fault Zone. Pure and Applied Geophysics, 173(12), 4189–4201.

Ihmlé, P. F. (1996). Monte Carlo slip inversion in the frequency domain:: Application to the 1992 Nicaragua Slow Earthquake. Geophys. Res. Lett., 23(9), 913–916.

Ihmlé, P. F., Gomez, J., Martin, Heinrich, P., & Guibourg, S. (1998). The 1996 Peru tsunamigenic earthquake: Broadband source process. Geophys. Res. Lett., 25(14), 2691–2694.

Jacob, J., Dyment, J. & Yatheesh, V. (2014). Revisiting the structure, age, and evolution of the Wharton Basin to better understand subduction under Indonesia: Journal of Geophysical Research, v. 119, p. 169–190.

Japan Agency for Marine-Earth Science and Technology (2016) Data and Sample Research System for Whole Cruise Information in JAMSTEC (DARWIN). http://www.godac.jamstec.go.jp/darwin/, Accessed on 2019-03-01.

Johnson, J. M., & Satake, K. (1997). Estimation of seismic moment and slip distribution of the April 1, 1946, Aleutian tsunami earthquake. Journal of Geophysical Research: Solid Earth, 102(B6), 11765–11774.

Kanamori, H. (1972). Mechanism of tsunami earthquakes. Physics of the Earth and Planetary Interiors, 6(5), 346–359.

Kanamori, H., & Kikuchi, M. (1993). The 1992 Nicaragua earthquake: a slow tsunami earthquake associated with subducted sediments. Nature, 361(6414), 714.

Kanamori, H., Rivera, L., & Lee, W. H. K. (2010). Historical seismograms for unravelling a mysterious earthquake: The 1907 Sumatra Earthquake. Geophysical Journal International, 183(1), 358–374.

Kelleher, J., & McCann, W. (1976). Buoyant Zones, Great Earthquakes, and Unstable Boundaries of Subduction. J. Geophys. Res., 81(26), 4885–4896.

Kim, S.-S., & Wessel, P. (2011). New global seamount census from altimetry-derived gravity data. Geophysical Journal International, 186(2), 615–631.

Kläschen, D., Belykh, I., Gnibidenko, H., Patrikeyev, S., & Huene, R. (1994). Structure of the Kuril Trench from seismic reflection records. Journal of Geophysical Research: Solid Earth, 99(B12), 24173-24188.

Kodaira, S., Takahashi, N., Nakanishi, A., Miura, S., & Kaneda, Y. (2000). Subducted Seamount Imaged in the Rupture Zone of the 1946 Nankaido Earthquake. Science, 289(5476), 104–106.

Kodaira, S., Nakamura, Y., Yamamoto, Y., Obana, K., Fujie, G., No, T., ... & Miura, S. (2017). Depth-varying structural characters in the rupture zone of the 2011 Tohoku-oki earthquake. Geosphere, 13(5), 1408-1424.

Koketsu, K., Yokota, Y., Nishimura, N., Yagi, Y., Miyazaki, S., Satake, K., … Okada, T. (2011). A unified source model for the 2011 Tohoku earthquake. Earth and Planetary Science Letters, 310(3), 480–487.

Kopp, H., & Kukowski, N. (2003). Backstop geometry and accretionary mechanics of the Sunda margin. Tectonics, 22(6), 1072.

Kopp, H., Flueh, E. R., Petersen, C. J., Weinrebe, W., Wittwer, A., & Scientists, M. (2006). The Java margin revisited: Evidence for subduction erosion off Java. Earth and Planetary Science Letters, 242, 130–142.

Kopp, H., Weinrebe, W., Ladage, S., Barckhausen, U., Klaeschen, D., Flueh, E. R., ... & Papenberg, C. (2008). Lower slope morphology of the Sumatra trench system. Basin Research, 20(4), 519-529.

Lange, D., Geersen, J., Barrientos, S., Moreno, M., Grevemeyer, I., Contreras-Reyes, E., & Kopp, H. (2016). Aftershock seismicity and tectonic setting of the 2015 September 16 Mw 8.3 Illapel earthquake, Central Chile. Geophysical Journal International, 206(2), 1424–1430.

Lay, T., & Bilek, S. (2007). Anomalous Earthquake Ruptures at Shallow Depths on Subduction Zone Megathrusts. The Seismogenic Zone of Subduction Thrust Faults, 476.

Lay, T., Li, L., & Cheung, K. F. (2016). Modeling tsunami observations to evaluate a proposed late tsunami earthquake stage for the 16 September 2015 Illapel, Chile, Mw 8.3 earthquake. Geophysical Research Letters, 43(15), 2016GL070002.

Lay, T., Ammon, C. J., Kanamori, H., Yamazaki, Y., Cheung, K. F., & Hutko, A. R. (2011). The 25 October 2010 Mentawai tsunami earthquake (Mw 7.8) and the tsunami hazard presented by shallow megathrust ruptures. Geophysical Research Letters, 38(6), L06302.

Lay, T., & Kanamori, H. (2011). Insights from the great 2011 Japan earthquake. Physics Today, 64(12), 33–39.

Lee, S.-J., Yeh, T.-Y., Lin, T.-C., Lin, Y.-Y., Song, T.-R. A., & Huang, B.-S. (2016). Two-stage composite megathrust rupture of the 2015 Mw8.4 Illapel, Chile, earthquake identified by spectral-element inversion of teleseismic waves. Geophysical Research Letters, 43(10), 2016GL068843.

Lüschen, E., Müller, C., Kopp, H., Engels, M., Lutz, R., Planert, L., … Djajadihardja, Y. S. (2011). Structure, evolution and tectonic activity of the eastern Sunda forearc, Indonesia, from marine seismic investigations. Tectonophysics, 508, 6–21.

McAdoo, B.G., Dengler, L., Prasetya, G., & Titov, V. (2006). How an oral history saved thousands on Indonesia's Simeulue Island during the December 2004 and March 2005 tsunamis. Earthquake Spectra, 22, S661–S669.

McIntosh, K. D., Silver, E. a, Ahmed, I., Berhorst, A., Ranero, C. R., Kelly, R. K., & Flueh, E. R. (2007). The Nicaragua Convergent Margin: Seismic Reflection Imaging of the Source of a Tsunami Earthquake. University of British Columbia Press.

McSaveney, E. (2006). 'Tsunamis - 20th-century and recent tsunamis', Te Ara - the Encyclopedia of New Zealand, http://www.TeAra.govt.nz/en/tsunamis/page-3 (accessed 4 January 2018)

Monecke, K., Finger, W., Klarer, D., Kongko, W., McAdoo, B.G., & Moore, A.L. (2008). A 1,000-year sediment record of tsunami recurrence in northern Sumatra, Nature, 455, 1232–1234.

Miller, J. J., von Huene, R. E., & Ryan, H. F. (2014). The 1946 Unimak Tsunami Earthquake Area: revised tectonic structure in reprocessed seismic images and a suspect near field tsunami source (USGS Numbered Series No. 2014–1024) (p. 22). Reston, VA: U.S. Geological Survey.

Mitchell, J.S., Mackay, K.A., Neil, H.L., Mackay, E.J., Pallentin, A., & Notman P. (2012). Undersea New Zealand, 1:5,000,000. NIWA Chart, Miscellaneous Series No. 92

Müller, R. D., Sdrolias, M., Gaina, C., & Roest, W. R. (2008). Age, spreading rates, and spreading asymmetry of the world's ocean crust. Geochemistry, Geophysics, Geosystems, 9(4), Q04006.

National Geophysical Data Center / World Data Service (NGDC/WDS): Global Historical Tsunami Database. National Geophysical Data Center, NOAA. doi:10.7289/V5PN93H7 [access date: 04/2018]

Newcomb, K. R., & McCann, W. R. (1987). Seismic history and seismotectonics of the Sunda arc. Journal of Geophysical Research, 92, 421–439.

Nishenko, S. P. (1991). Circum-Pacific seismic potential: 1989–1999. Pure and Applied Geophysics, 135(2), 169–259.

Okal, E. A., & Newman, A. V. (2001). Tsunami earthquakes: the quest for a regional signal. Physics of the Earth and Planetary Interiors, 124(1), 45–70.

Okal, E. A., Synolakis, C. E., Fryer, G. J., Heinrich, P., Borrero, J. C., Ruscher, C., … Rousseau, D. (2002). A Field Survey of the 1946 Aleutian Tsunami in the Far Field. Seismological Research Letters, 73(4), 490–503.

Pautot, G., & Bourgois, J. (1986) SEAPERC cruise, RV Jean Charcot.

Pedley, K. L., Barnes, P. M., Pettinga, J. R., & Lewis, K. B. (2010). Seafloor structural geomorphic evolution of the accretionary frontal wedge in response to seamount subduction, Poverty Indentation, New Zealand. Marine Geology, 270(1), 119–138.

Pelayo, A. M., & Wiens, D. A. (1990). The November 20,1960 Peru Tsunami Earthquake: Source mechanism of a slow event. Geophysical Research Letters, 17(6), 661–664.

Pelayo, A. M., & Wiens, D. A. (1992). Tsunami earthquakes: Slow thrust-faulting events in the accretionary wedge. Journal of Geophysical Research: Solid Earth, 97(B11), 15321–15337.

Polet, J., & Kanamori, H. (2000). Shallow subduction zone earthquakes and their tsunamigenic potential. Geophysical Journal International, 142(3), 684–702.

Poli, P., Maksymowicz, A., & Ruiz, S. (2017). The Mw 8.3 Illapel earthquake (Chile): Preseismic and postseismic activity associated with hydrated slab structures. Geology, 45(3), 247–250.

Prince, R. A., & Kulm, L. D. (1975). Crustal rupture and the initiation of imbricate thrusting in the Peru-Chile Trench. GSA Bulletin, 86(12), 1639–1653.

Ruff, L.J. (1989), Do trench sediments affect great earthquake occurrence in subduction zones?, Pure and Applied Geophysics, v. 129, p. 263–282.

Ruh, J. B., Sallarès, V., Ranero, C. R., & Gerya, T. (2016). Crustal deformation dynamics and stress evolution during seamount subduction: High-resolution 3-D numerical modeling. Journal of Geophysical Research: Solid Earth, 121(9), 6880–6902.

Ryan, W. B. F., Carbotte, S. M., Coplan, J. O., O'Hara, S., Melkonian, A., Arko, R., … Zemsky, R. (2009). Global Multi-Resolution Topography synthesis. Geochem. Geophys. Geosyst., 10(3).

Saffer, D. M., & Wallace, L. M. (2015). The frictional, hydrologic, metamorphic and thermal habitat of shallow slow earthquakes. Nature Geoscience, 8(8), 594.

Sallarès, V., Meléndez, A., Prada, M., Ranero, C. R., McIntosh, K., & Grevemeyer, I. (2013). Overriding plate structure of the Nicaragua convergent margin: Relationship to the seismogenic zone of the 1992 tsunami earthquake. Geochemistry, Geophysics, Geosystems, 14(9), 3436–3461.

Sandwell, D. T., Müller, R. D., Smith, W. H. F., Garcia, E., & Francis, R. (2014). New global marine gravity model from CryoSat-2 and Jason-1 reveals buried tectonic structure. Science, 346(6205), 65–67.

Satake, K. (1994). Mechanism of the 1992 Nicaragua Tsunami Earthquake. Geophys. Res. Lett., 21(23), 2519–2522.

Satake, K., & Tanioka, Y. (1999). Sources of Tsunami and Tsunamigenic Earthquakes in Subduction Zones. In J. Sauber & R. Dmowska (Eds.), Seismogenic and Tsunamigenic Processes in Shallow Subduction Zones (pp. 467–483). Basel: Birkhäuser Basel.

Scholl, D. W., Kirby, S. H., von Huene, R., Ryan, H., Wells, R. E., & Geist, E. L. (2015). Great (≥ Mw8. 0) megathrust earthquakes and the subduction of excess sediment and bathymetrically smooth seafloor. Geosphere, 11(2), 236-265.

Scholz, C. H., & Campos, J. (2012). The seismic coupling of subduction zones revisited. J. Geophys. Res., 117(B5), B05310.

Şen, A. T., Cesca, S., Lange, D., Dahm, T., Tilmann, F., & Heimann, S. (2015). Systematic changes of earthquake rupture with depth: a case study from the 2010 M w 8.8 Maule, Chile, earthquake aftershock sequence. Bulletin of the Seismological Society of America, 105(5), 2468-2479.

Seno, T. (2000). The 21 September, 1999 Chichi earthquake in Taiwan: implications for tsunami earthquakes, Terr. Atmos. Ocean Sci., 11, 701–708.

Seno, T., & Hirata, K. (2007). Did the 2004 Sumatra–Andaman earthquake involve a component of tsunami earthquakes? Bulletin of the Seismological Society of America, 97(1A), S296-S306.

Shulgin, A., Kopp, H., Mueller, C., Planert, L., Lueschen, E., Flueh, E. R., & Djajadihardja, Y. (2011). Structural architecture of oceanic plateau subduction offshore Eastern Java and the potential implications for geohazards. Geophysical Journal International, 184(1), 12–28.

Singh, S. C., Hananto, N., Mukti, M., Permana, H., Djajadihardja, Y., & Harjono, H. (2011). Seismic images of the megathrust rupture during the 25th October 2010 Pagai earthquake, SW Sumatra: Frontal rupture and large tsunami. Geophysical Research Letters, 38(16).

Singh, S. C., Hananto, N., Qin, Y., Leclerc, F., Avianto, P., Tapponnier, P. E., ... & Sieh, K. (2017). The discovery of a conjugate system of faults in the Wharton Basin intraplate deformation zone. Science advances, 3(1), e1601689.

Tanioka, Y., Ruff, L., & Satake, K. (1997). What controls the lateral variation of large earthquake occurrence along the Japan Trench? Island Arc, 6(3), 261–266.

Tanioka, Y., & Seno, T. (2001). Sediment effect on tsunami generation of the 1896 Sanriku tsunami earthquake. Geophysical Research Letters, 28(17), 3389-3392.

Titov, V., Rabinovich, A. B., Mofjeld, H. O., Thomson, R. E., & González, F. I. (2005). The Global Reach of the 26 December 2004 Sumatra Tsunami. Science, 309(5743), 2045–2048.

Tsuru, T., Park, J.O., Takahashi, N., Kodaira, S., Kido, Y., Kaneda, Y., & Kono, Y. (2000). Tectonic features of the Japan Trench convergent margin off Sanriku, northeastern Japan, revealed by multichannel seismic reflection data. Journal of Geophysical Research, v. 105, B7, p. 16,403–16,413.

Wang, K., & Bilek, S. L. (2011). Do subducting seamounts generate or stop large earthquakes? Geology, 39(9), 819–822.

Wang, K., & Bilek, S. L. (2014). Invited review paper: Fault creep caused by subduction of rough seafloor relief. Tectonophysics, 610, 1–24.

Wessel, P., Matthews, K. J., Müller, R. D., Mazzoni, A., Whittaker, J. M., Myhill, R., & Chandler, M. T. (2015). Semiautomatic fracture zone tracking. Geochemistry, Geophysics, Geosystems, 16(7), 2462-2472.

Yamazaki, Y., Cheung, K. F., & Lay, T. (2018). A Self-Consistent Fault Slip Model for the 2011 Tohoku Earthquake and Tsunami. Journal of Geophysical Research: Solid Earth, 123(2), 1435-1458.

Date	Name	Epicenter Location	Mw	Ms	Tsunami run-up max. [m]	Fatalities	Bathymetric data
15.06.1896	Sanriku	144 39.5	8.0	7.2	38	27122	R/V KAIREI KR11-E05, KR13-11; GMRT; SRTM15+
04.01.1907	Sumatra	96.11 +/-1° 2.48 +/-1°		7.8		400	R/V SONNE SO137, SO139, SO184, SO186, SO198, SO200; GMRT; SRTM15+
01.04.1946	Aleutian	-163.19 53.32	8.2	7.4	42	167	R/V SONNE SO96, SO97; R/V Roger Revelle KRUS03RR; GMRT; SRTM15+
25.03.1947	Poverty Bay	178.8 -38.85	7.1	7.2	10	0	R/V SONNE SO135, SO168, SO191; GMRT; NZ Reg. Bathymetry (2016)
17.05.1947	Tokomaru Bay	178.87 -38.42	7.0	7.2	6	0	R/V SONNE SO135, SO168, SO191; GMRT; NZ Reg. Bathymetry (2016)
20.11.1960	Peru	-80.9 -6.72	7.6	6.8	9	66	R/V METEOR M77; R/V SONNE SO146, SO147, SO162, SO209; R/V Jean Charcot (SEAPERC); GMRT; SRTM15+
20.10.1963	Kuril	150.7 44.7	7.8	7.2	15	0	GMRT; SRTM15+
10.06.1975	Kuril	147.635 43.074	7.5	7.0	5	0	GMRT; SRTM15+
02.09.1992	Nicaragua	-87.38 11.75	7.7	7.2	9	170	R/V Roger Revelle DELV02RR; R/V Maurice Ewing 0005, 0104, 0412, 9502; R/V SONNE SO76, SO81, SO107, SO144, SO150, SO163, SO173; GMRT; SRTM15+
02.06.1994	Java	113.04 -10.28	7.8	7.2	14	238	R/V SONNE SO137, SO138, SO139, SO176, SO179, SO184, SO190; SRTM15+
21.02.1996	Peru	-79.59 -9.59	7.5	6.6	5	12	R/V METEOR M77; R/V SONNE SO146, SO147, SO162, SO209; R/V Jean Charcot (SEAPERC); GMRT; SRTM15+
17.07.2006	Java	107.39 -9.26	7.8	7.2	21	802	R/V SONNE SO137, SO138, SO139, SO176, SO179, SO184, SO190; SRTM15+
25.10.2010	Mentawai	100.11 -3.48	7.8	7.3	17	431	R/V SONNE SO137, SO139, SO184, SO186, SO198, SO200; GMRT; SRTM15+

Table 1. *List of tsunami earthquakes and their characteristics since 1896. Information on fatalities and tsunami-run-up from NGDC/WDC (2018). The sources for the bathymetric data shown in Figures 2-8 are also listed.*

Name	Convergence rate (cm/a)	Convergence obliquity [°] (90=orthogonal)	Age subducting plate [Ma]	Max sediment thickness in Trench [m]	Structure of subducting plate (max height of respective seafloor expression)
1896 Sanriku	9.2	77	131	<500	Horst-and-grabens (800 m)
1907 Sumatra	5.4	65	48	2000-2500	96° fracture-zone but uncertain location of epicenter
1946 Aleutian	6.7	67	56	1000	Horst-and-grabens (250 m) Seamounts (1500 m) Subducted seamounts (1500 m)
1947 Poverty Bay	4.4	50	120	1100	Ruatoria debris avalanche (1500 m high individual blocks) Seamounts (1500 m) Subducted seamounts (2500 m)
1947 Tokomaru Bay	4.4	50	120	1100	Ruatoria debris avalanche (1500 m blocks) Seamounts (1500 m) Subducted seamounts (2500 m)
1960 Peru	6.7	72	30	300-700	Horst-and-grabens (150 m) Seamounts (400 m) Trujillo Trough (1000 m)
1963 Kuril	9.0	51	116	<800	Horst-and-grabens (400 m) Individual seamounts (1400 m) Subducting seamount (1500 m)
1975 Kuril	9.1	50	120	<800	Horst-and-grabens (400 m) Two fracture-zones Individual seamounts (1800 m)
1992 Nicaragua	7.4	69	25	300-400	Horst-and-grabens (400 m) Seamounts (1300 m) Subducted seamounts
1994 Java	7.0	85	126	<500	Horst-and-grabens (300 m) Roo Rise (2500 m)
1996 Peru	6.9	73	35	0-500	Mendena Fracture Zone (1000 m)
2006 Java	7.0	81	106	0 - 1300	Trench perpendicular ridges (800 m) Seamounts (3500 m)
2010 Mentawai	5.9	53	77	~1100	Horst-and-grabens (200 m) Seamounts (3500 m)

Table 2. *Structural and morphological parameters for all tsunami earthquake regions. Ages of the subducting lithosphere after Müller et al. (2008). Rate and direction of plate-convergence after DeMets et al. (2010).*

Figure Captions

Figure 1. *Global occurrence of tsunami earthquakes since 1896.*

Figure 2. Tsunami earthquakes off Hokkaido and the Kurils. (*A) Bathymetric map of the marine forearc and the oceanic plate in the area of the 1896, 1963, and 1975 tsunami earthquakes. The spatial extent of the 1896 rupture area is estimated from Satake and Tanioka (1999). (B) Residual bathymetric map from Basset and Watts (2015A, 2015B). Please note that the map is mosaicked from two individual residual grids (divided by the dashed grey line). Values were calculated individually for the two grids. (C) Seismic line D19 (Kodaira et al., 2017). (D) Interpretive line-drawing of seismic line D19 (modified from Kodaira et al., 2017). (E) Seismic line 3 (Kläschen et al., 1994) (F) Interpretive line-drawing of seismic line 3 (modified from Kläschen et al., 1994).*

Figure 3. *Tsunami earthquakes off Sumatra.* (*A) Bathymetric map of the marine forearc and the oceanic plate in the area of the 1907 and 2010 tsunami earthquakes. Oceanic fracture-zones from Jacob et al. (2014). The spatial extent of the 2010 rupture area is estimated from Hill et al., 2012. SIM = Simeulue; NIA = Nias; SIB = Siberut; PAG = Pagai (B) Residual bathymetric map from Basset and Watts (2015A, 2015B). (C) Seismic line CGGV02020 (Singh et al., 2011). (D) Interpretive line-drawing of seismic line CGGV02020 (modified from Singh et al., 2011).*

Figure 4. *Tsunami earthquake off the Aleutians.* (*A) Bathymetric map of the marine forearc and the oceanic plate in the area of the 1946 tsunami earthquakes. The spatial extent of the rupture area is estimated from Satake and Tanioka (1999). (B) Residual bathymetric map from Basset and Watts (2015A, 2015B). (C) Seismic line Ewing 1237 (Miller et al., 2014). (D) Interpretive line-drawing of seismic line Ewing 1237 (modified from Miller et al., 2014; von Huene et al., 2016).*

Figure 5. *Tsunami earthquakes off New Zealand. (A) Bathymetric map of the marine forearc and the oceanic plate in the area of the 1947 Poverty Bay (PB) and Tokomaru Bay (TB) tsunami earthquakes. The spatial extent of the rupture area of the PB event is estimated from Bell et al. (2014). (B) Residual bathymetric map from Basset and Watts (2015A, 2015B). (C) Seismic line 05CM-04 (Barker et al., 2018). (D) Interpretive line-drawing of seismic line 05CM-04 (modified from Barker et al., 2018).*

Figure 6. *Tsunami earthquakes off Peru. (A) Bathymetric map of the marine forearc and the oceanic plate in the area of the 1960 and 1996 tsunami earthquake. The spatial extent of the 1996 rupture area is estimated from Ihmlé et al. (1998). (B) Residual bathymetric map from Basset and Watts (2015A, 2015B). (C) Interpretive line-drawing of seismic line 50 (modified from Huchon and Bourgois, 1990). (D) Interpretive line-drawing of seismic line 120 (modified from Huchon and Bourgois, 1990).*

Figure 7. *Tsunami earthquakes off Nicaragua. (A) Bathymetric map of the marine forearc and the oceanic plate in the area of the 1992 tsunami earthquake. The spatial extent of the rupture*

area is estimated from Satake and Tanioka (1999). Dashed red ellipses highlight the areas of largest moment release during the event (Ihmlé, 1996). (B) Residual bathymetric map from Basset and Watts (2015A, 2015B). (C) Seismic line NIC28 (McIntosh et al., 2007). (D) Interpretive line-drawing of seismic line NIC28 (modified from McIntosh et al., 2007).

Figure 8. *Tsunami earthquakes off Java. (A) Bathymetric map of the marine forearc and the oceanic plate in the area of the 1994 and 2006 tsunami earthquakes. The spatial extent of both rupture areas is estimated from Bilek and Engdahl (2007). (B) Residual bathymetric map from Basset and Watts (2015A, 2015B). (C) Trench parallel seafloor profile across the oceanic plate seaward of the rupture area of the 2006 event. (D) Seismic line BGR06-305 (Lüschen et al., 2011). (E) Interpretive line-drawing of seismic line BGR06-305 (modified from Lüschen et al., 2011; Shulgin et al., 2011).*

Figure 9. *Occurrence of tsunami earthquakes relative to trench sediment thickness (modified from Geersen et al., 2018). In sediment starved trenches the tectonic structure of the oceanic plate (e.g. spreading fabric) can be traced to the deformation front. In partly sediment filled trenches the tectonic structure of the oceanic plate might be masked by trench sediment but the trench outer slope is still visible as a morphologic feature. In sediment flooded trenches the trench outer slope is buried under sediment and not visible in bathymetric maps. This discrimination, however, only works for regions where the oceanic plate is not overprinted by large-scale topographic features such as basement ridges or oceanic plateaus. The rupture areas of some large and giant tsunamigenic earthquakes are also shown.*

Figure 10. *Conceptual model showing how subducting lower-plate relief influences the structural development of the plate-boundary adjacent to (A) sediment starved trenches and (B) sediment flooded trenches. The bulk of the upper-plate has been removed for simplification. Tsunami earthquakes may preferentially occur along shallow plate-boundaries where subducting lower-plate relief is not blanketed by subducting sediment.*

Highlights

I collated bathymetric data from active margins that experienced tsunami earthquakes

Tsunami earthquakes occurred where subducting relief is not blanketed by sediment

Tsunami earthquakes are linked to structurally and lithological complex megathrusts

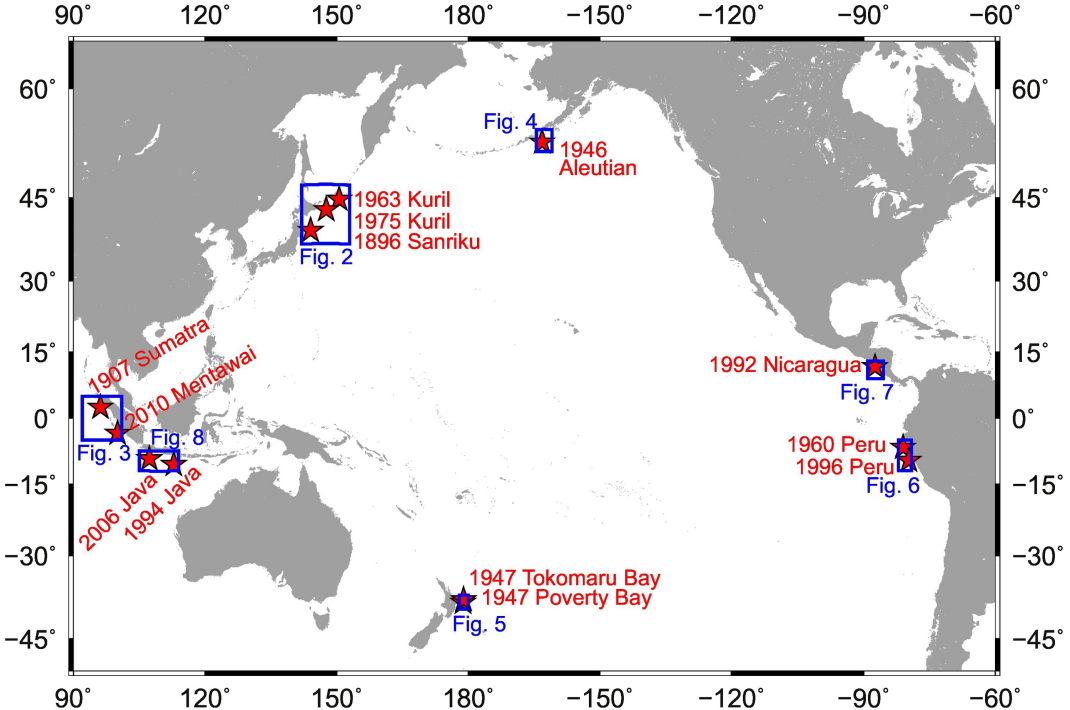
90°
120°
150°
180°
−150°
−120°
−90°
−60°
60°
45°
30°
15°
0°
−15°
−30°
−45°
Fig. 4
1946
Aleutian
1963 Kuril
1975 Kuril
1896 Sanriku
Fig. 2
1907 Sumatra
2010 Mentawai
Fig. 3
Fig. 8
2006 Java
1994 Java
1992 Nicaragua
Fig. 7
1960 Peru
1996 Peru
Fig. 6
1947 Tokomaru Bay
1947 Poverty Bay
Fig. 5

Figure 1

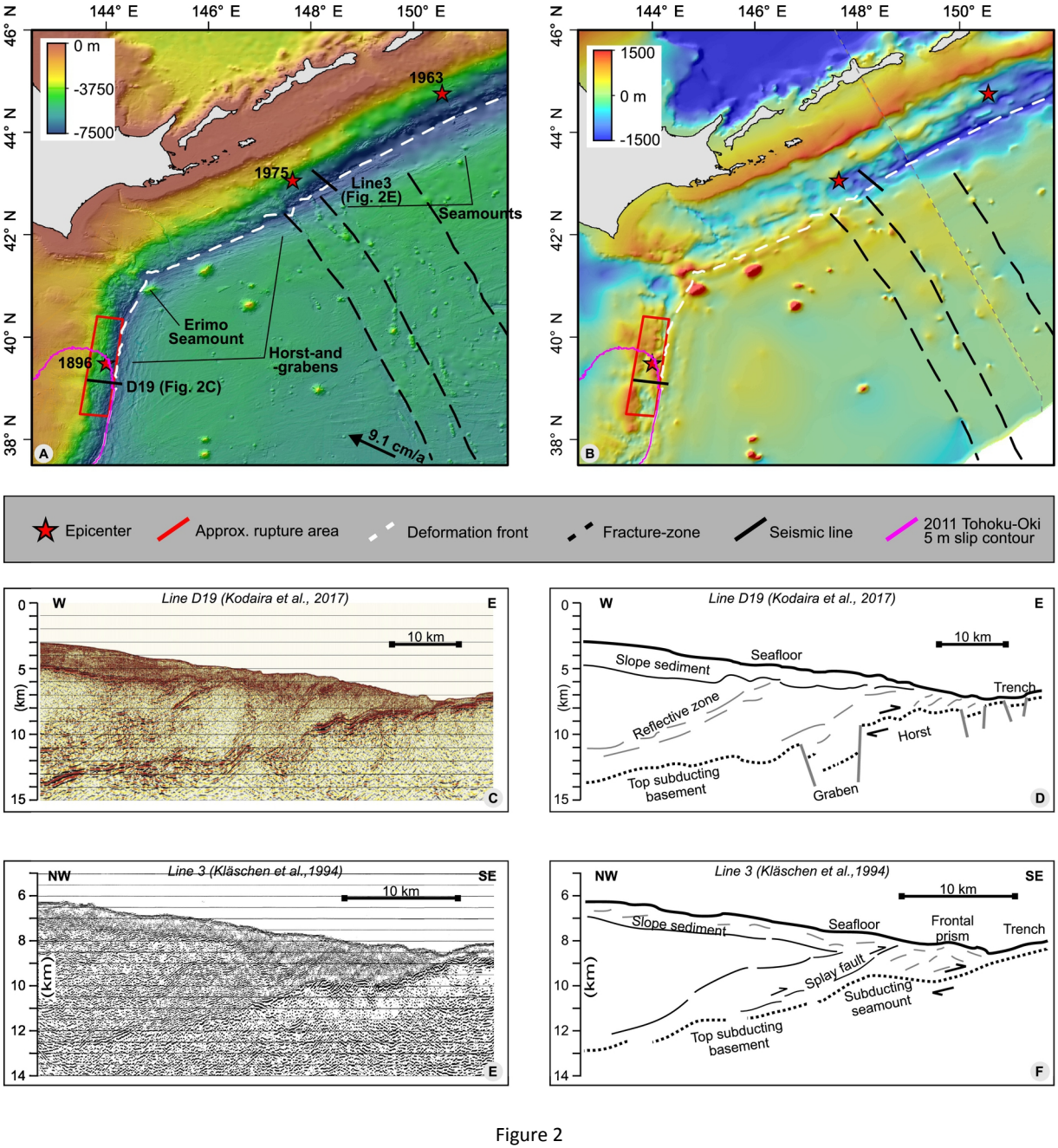
144° E
146° E
148° E
150° E
46° N
44° N
42° N
40° N
38° N
0 m
-3750
-7500
1963
1975
Line3
(Fig. 2E)
Seamounts
Erimo
Seamount
Horst-and
-grabens
1896
D19 (Fig. 2C)
9.1 cm/a
A
1500
0 m
-1500
B
Epicenter
Approx. rupture area
Deformation front
Fracture-zone
Seismic line
2011 Tohoku-Oki
5 m slip contour
W
E
Line D19 (Kodaira et al., 2017)
10 km
(km)
C
Slope sediment
Seafloor
Reflective zone
Trench
Horst
Top subducting
basement
Graben
D
NW
SE
Line 3 (Kläschen et al.,1994)
Slope sediment
Seafloor
Frontal
prism
Trench
Splay fault
Subducting
seamount
Top subducting
basement
E
F

Figure 2

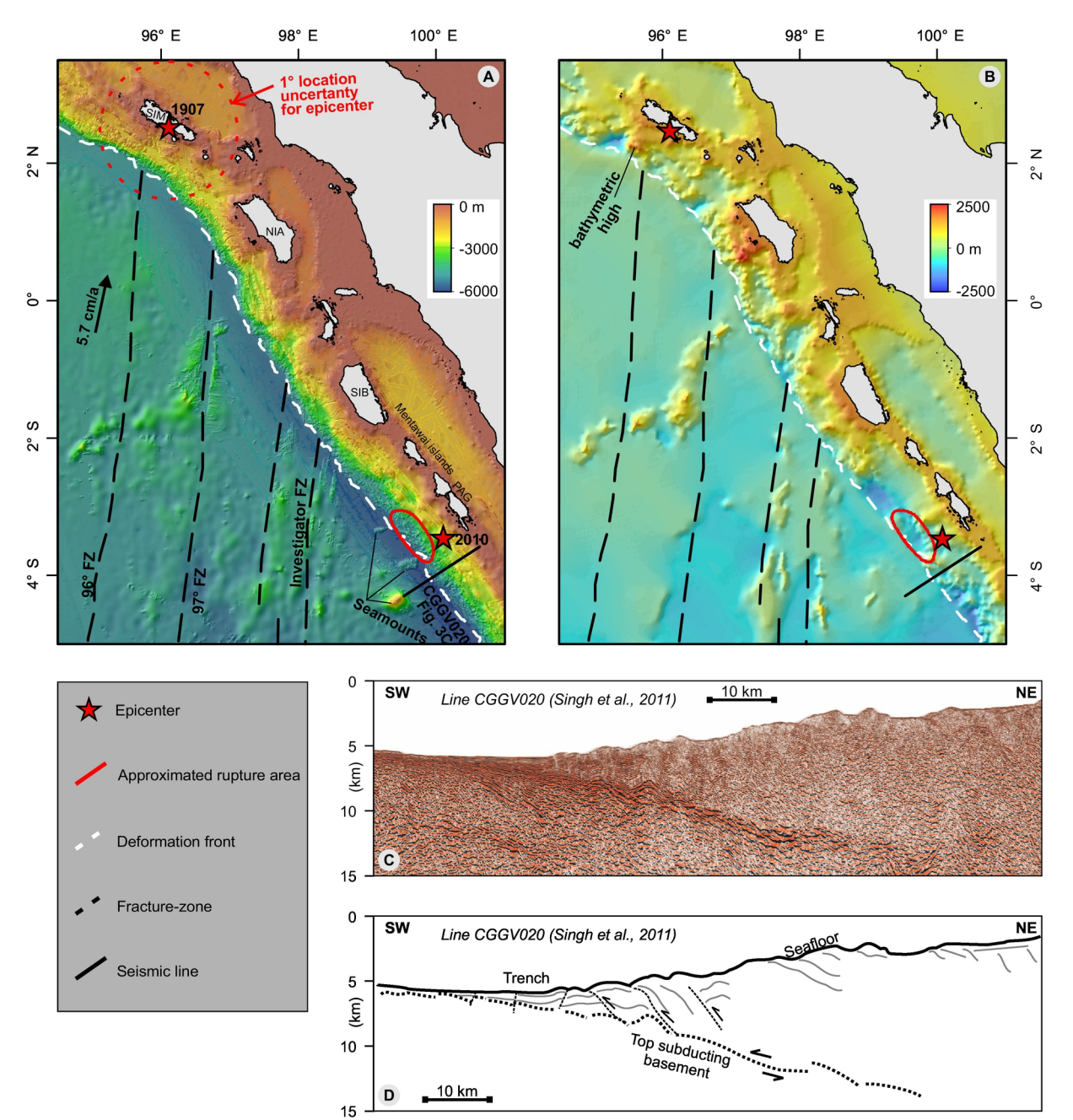
96° E
98° E
100° E
2° N
0°
2° S
4° S
A
B
1° location uncertanty for epicenter
1907
2010
SIM
NIA
SIB
Mentawai islands
PAG
5.7 cm/a
96° FZ
97° FZ
Investigator FZ
Seamounts
CGGV020
Fig. 3C
0 m
-3000
-6000
2500
-2500
bathymetric high
Epicenter
Approximated rupture area
Deformation front
Fracture-zone
Seismic line
SW
NE
Line CGGV020 (Singh et al., 2011)
10 km
(km)
C
Trench
Seafloor
Top subducting basement
D

Figure 3

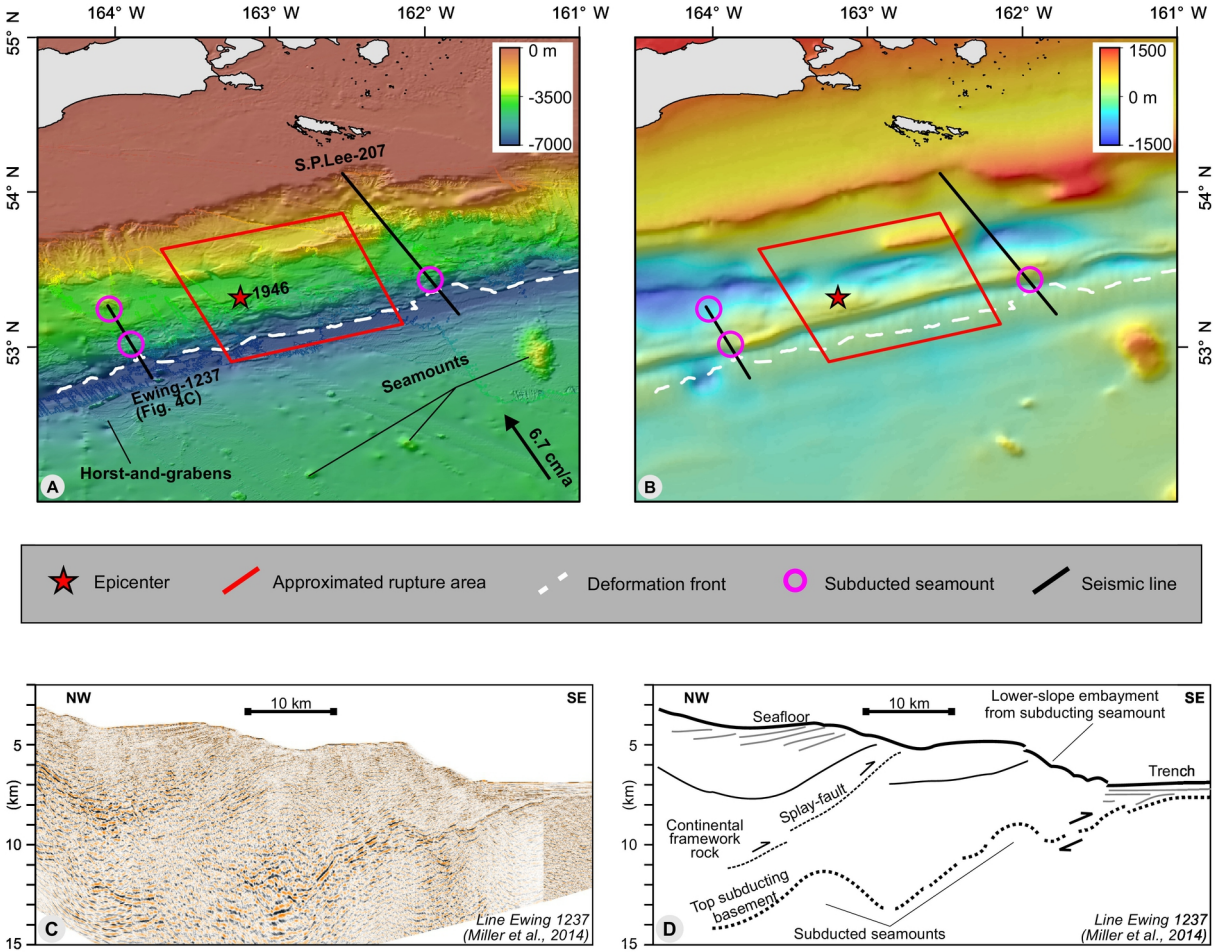
164° W
163° W
162° W
161° W
55° N
54° N
53° N
0 m
-3500
-7000
S.P.Lee-207
1946
Ewing-1237
(Fig. 4C)
Seamounts
6.7 cm/a
Horst-and-grabens
A
1500
0 m
-1500
B
Epicenter
Approximated rupture area
Deformation front
Subducted seamount
Seismic line
NW
SE
10 km
5
10
15
(km)
C
Line Ewing 1237
(Miller et al., 2014)
Seafloor
Lower-slope embayment
from subducting seamount
Trench
Splay-fault
Continental
framework
rock
Top subducting
basement
Subducted seamounts
D

Figure 4

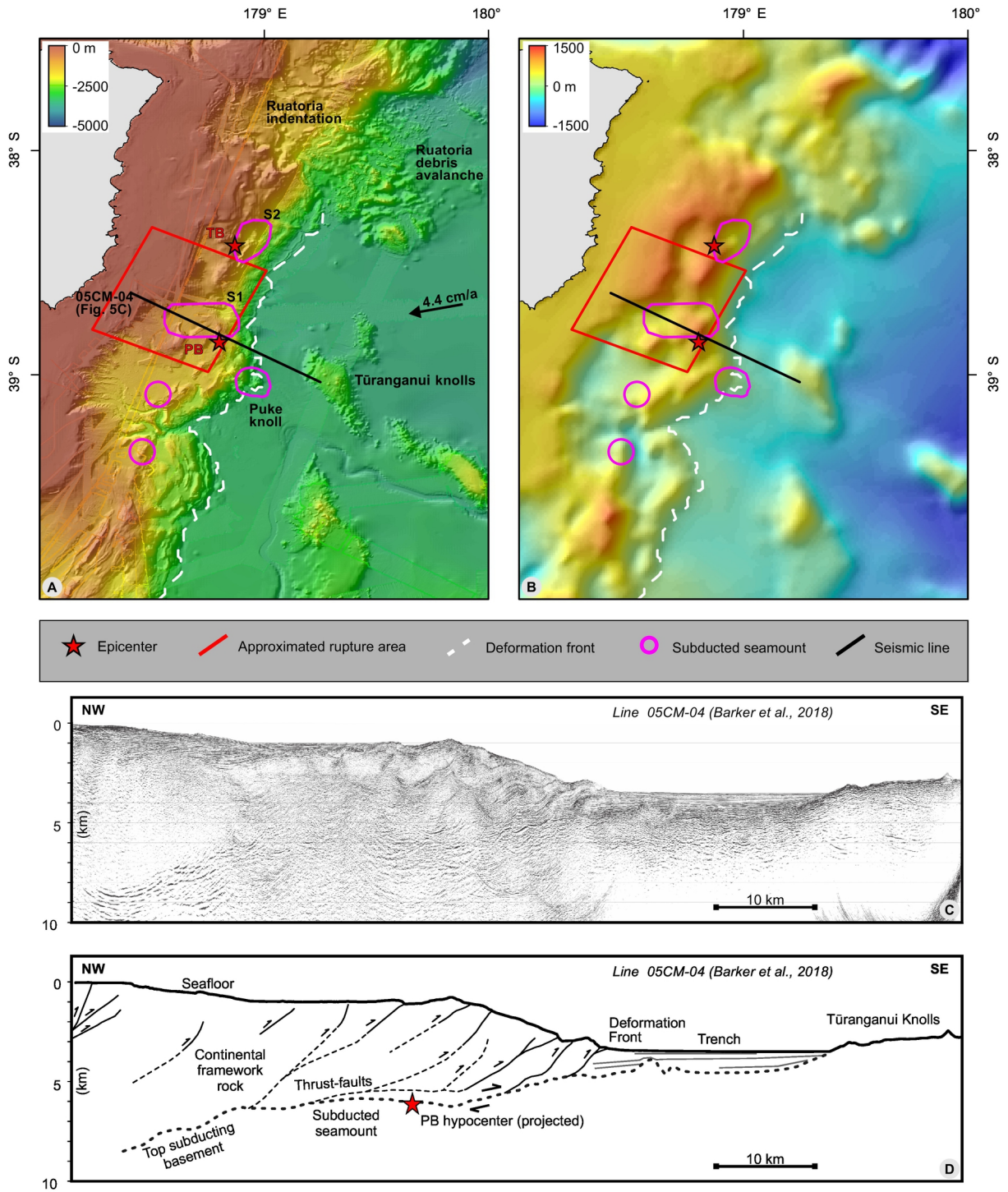
179° E
180°
38° S
39° S
0 m
-2500
-5000
Ruatoria indentation
Ruatoria debris avalanche
S2
TB
S1
PB
05CM-04 (Fig. 5C)
4.4 cm/a
Tūranganui knolls
Puke knoll
A
1500
0 m
-1500
B
Epicenter
Approximated rupture area
Deformation front
Subducted seamount
Seismic line
NW
SE
Line 05CM-04 (Barker et al., 2018)
(km)
10 km
C
Seafloor
Continental framework rock
Thrust-faults
Subducted seamount
PB hypocenter (projected)
Top subducting basement
Deformation Front
Trench
Tūranganui Knolls
D

Figure 5

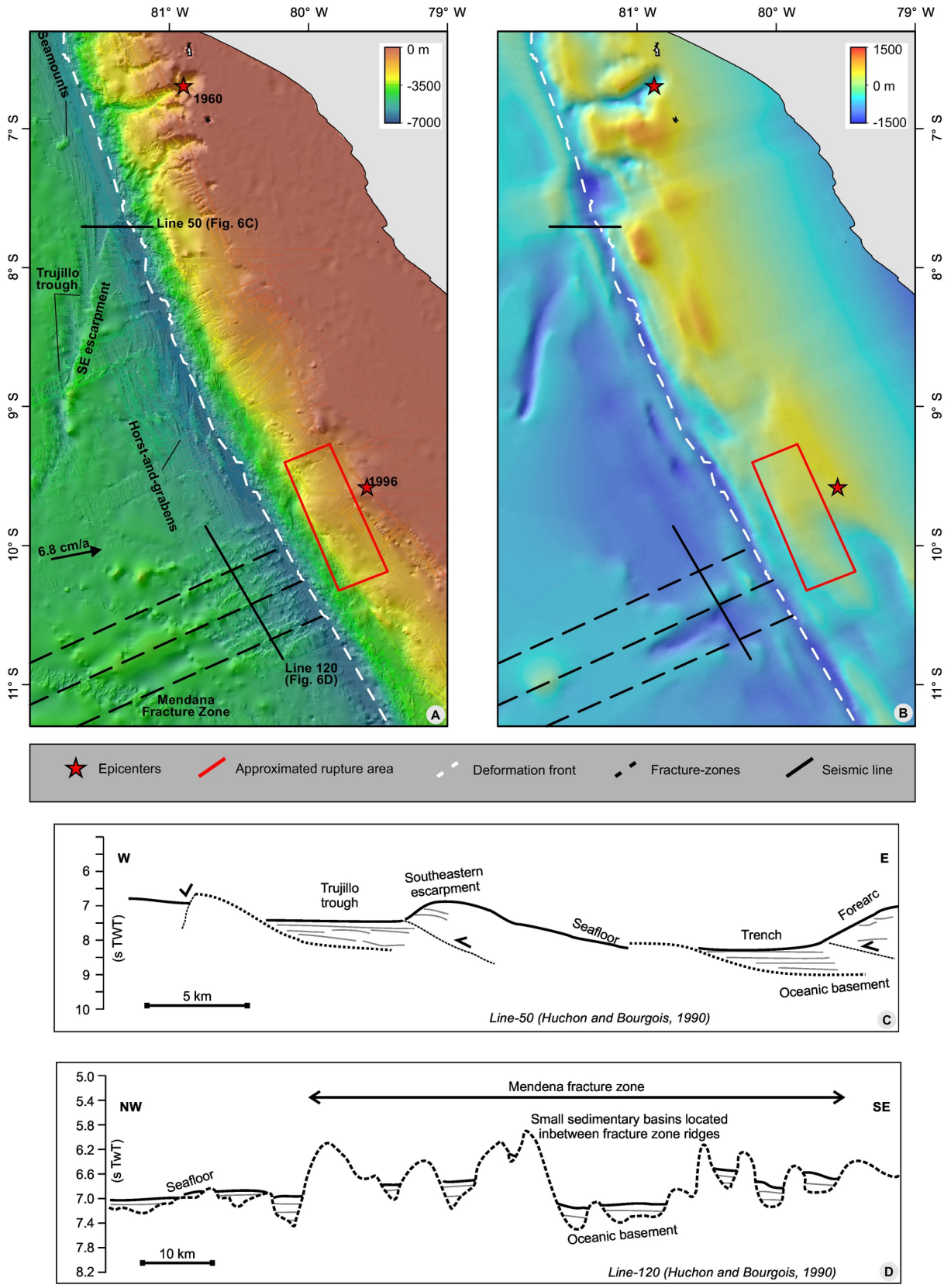
81° W
80° W
79° W
7° S
8° S
9° S
10° S
11° S
Seamounts
1960
0 m
-3500
-7000
Line 50 (Fig. 6C)
Trujillo trough
SE escarpment
Horst-and-grabens
1996
6.8 cm/a
Line 120 (Fig. 6D)
Mendana Fracture Zone
A
1500
0 m
-1500
B
Epicenters
Approximated rupture area
Deformation front
Fracture-zones
Seismic line
W
E
(s TWT)
Trujillo trough
Southeastern escarpment
Seafloor
Trench
Forearc
Oceanic basement
5 km
Line-50 (Huchon and Bourgois, 1990)
C
NW
SE
Mendena fracture zone
Small sedimentary basins located inbetween fracture zone ridges
(s TwT)
Seafloor
Oceanic basement
10 km
Line-120 (Huchon and Bourgois, 1990)
D

Figure 6

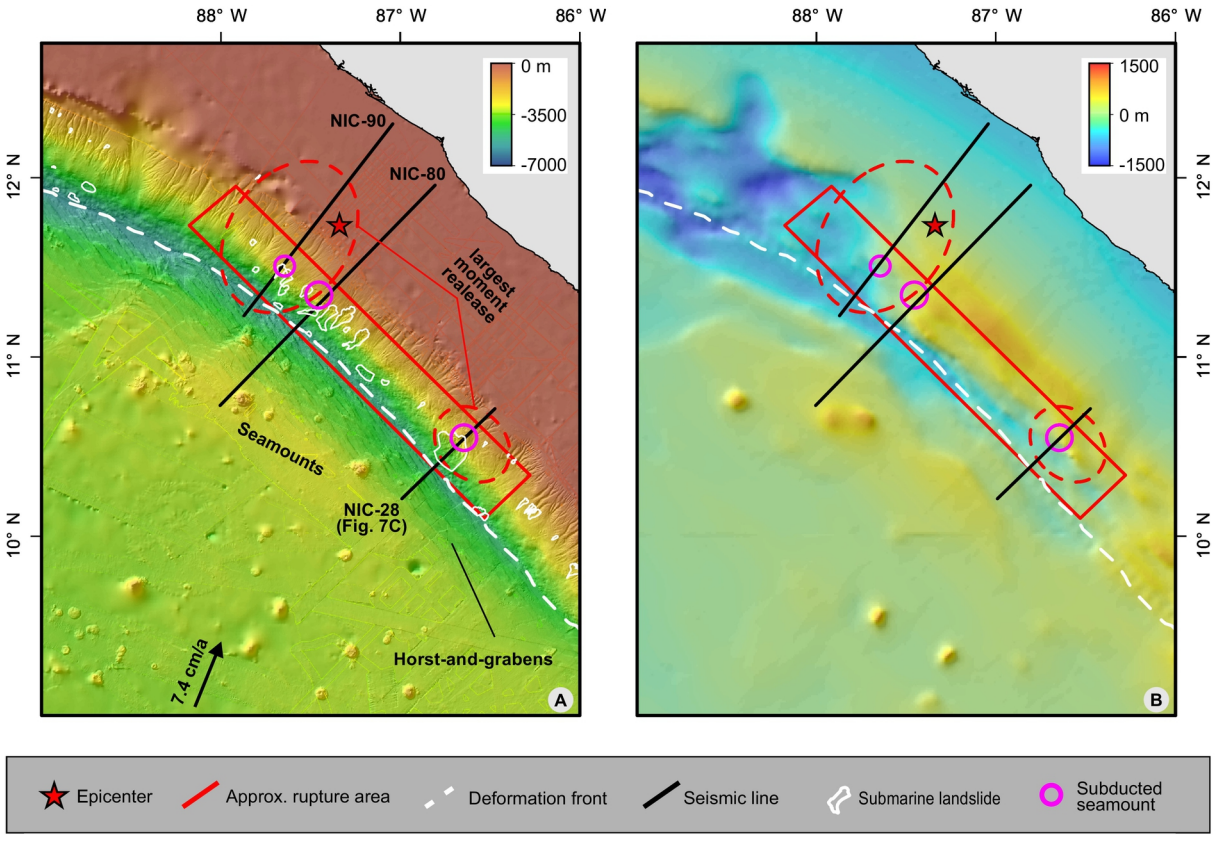
88° W
87° W
86° W
12° N
11° N
10° N
0 m
-3500
-7000
NIC-90
NIC-80
largest moment realease
Seamounts
NIC-28 (Fig. 7C)
Horst-and-grabens
7.4 cm/a
A
1500
0 m
-1500
B
Epicenter
Approx. rupture area
Deformation front
Seismic line
Submarine landslide
Subducted seamount
SW
NE
10 km
Line NIC28 (McIntosh et al., 2007)
(s TwT)
0
2
4
6
8
C
Seafloor
Continental framework rock
Trench
Top subducting basement
Subducted seamount
D

Figure 7

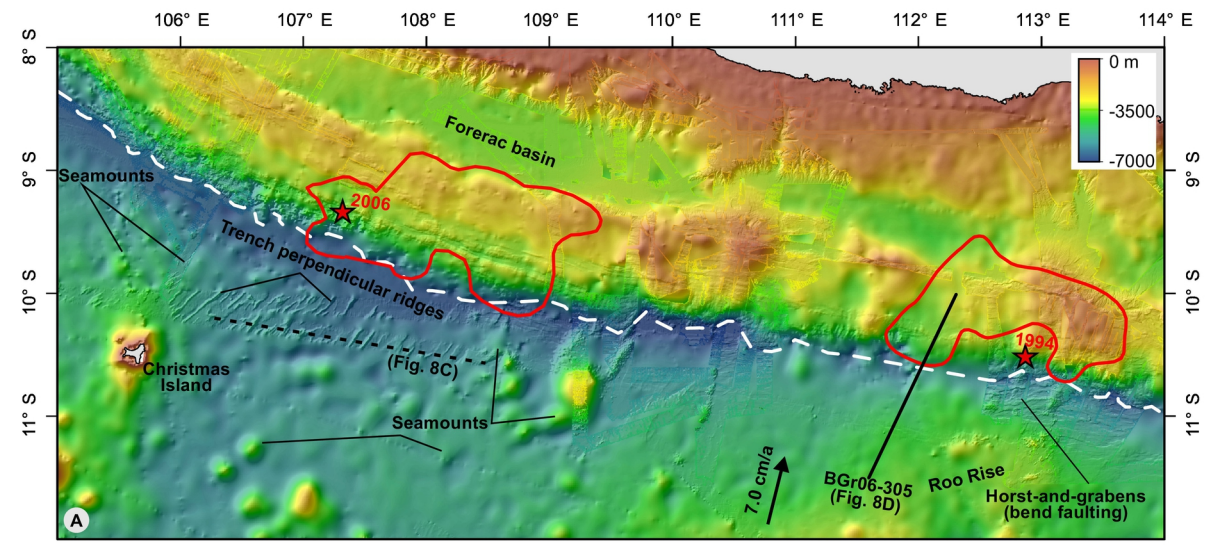
106° E
107° E
108° E
109° E
110° E
111° E
112° E
113° E
114° E
8° S
9° S
10° S
11° S
0 m
-3500
-7000
Forerac basin
Seamounts
2006
Trench perpendicular ridges
(Fig. 8C)
Christmas Island
Seamounts
1994
7.0 cm/a
BGr06-305 (Fig. 8D)
Roo Rise
Horst-and-grabens (bend faulting)
A

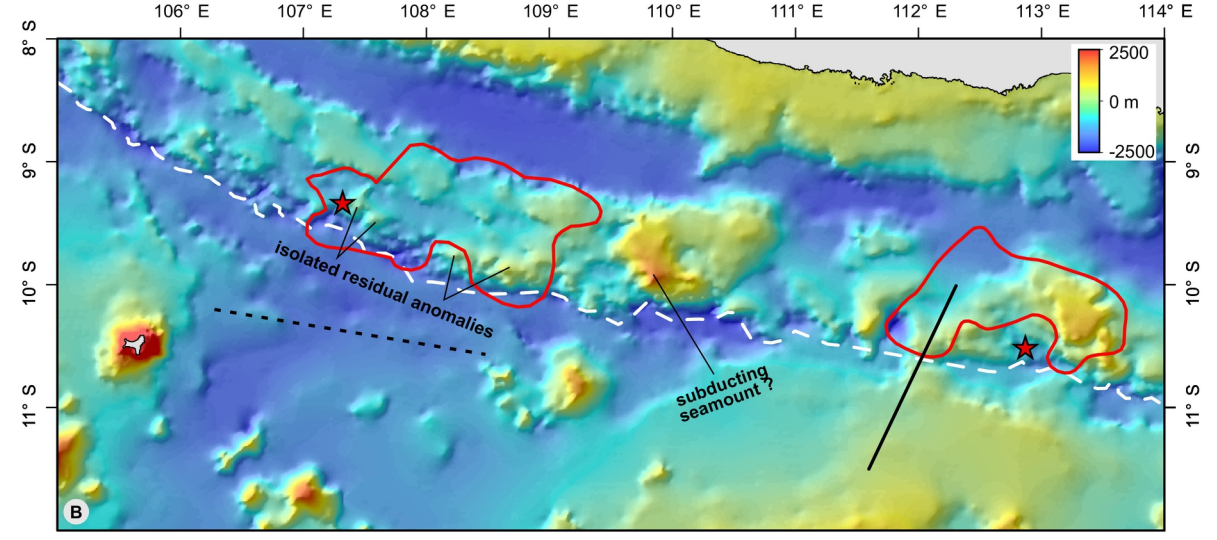
106° E
107° E
108° E
109° E
110° E
111° E
112° E
113° E
114° E
8° S
9° S
10° S
11° S
2500
0 m
-2500
isolated residual anomalies
subducting seamount ?
B

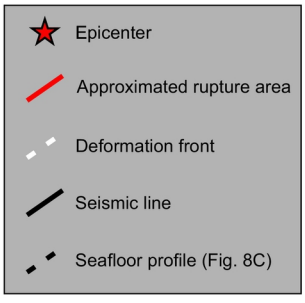
Epicenter
Approximated rupture area
Deformation front
Seismic line
Seafloor profile (Fig. 8C)

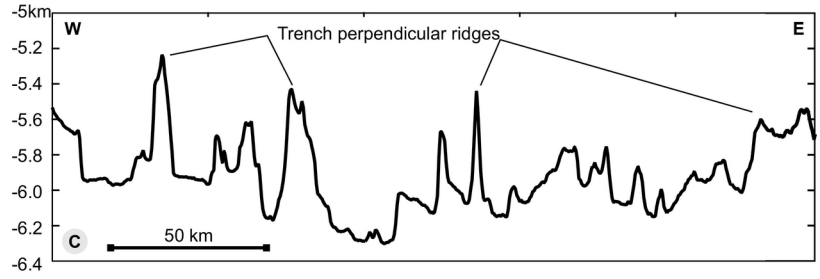
-5km
-5.2
-5.4
-5.6
-5.8
-6.0
-6.2
-6.4
W
E
Trench perpendicular ridges
C
50 km

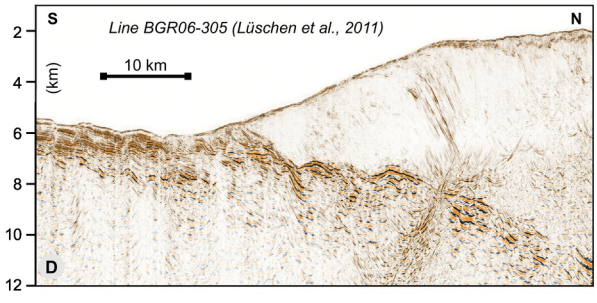
S
N
Line BGR06-305 (Lüschen et al., 2011)
10 km
(km)
2
4
6
8
10
12
D

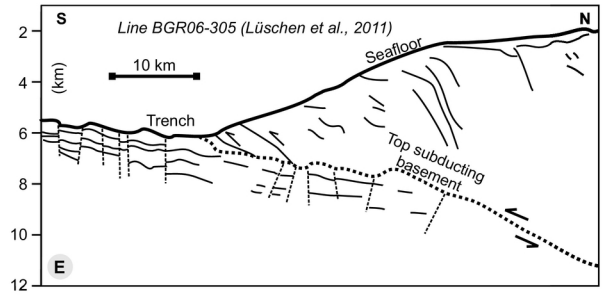
S
N
Line BGR06-305 (Lüschen et al., 2011)
10 km
(km)
Seafloor
Trench
Top subducting basement
2
4
6
8
10
12
E

Figure 8

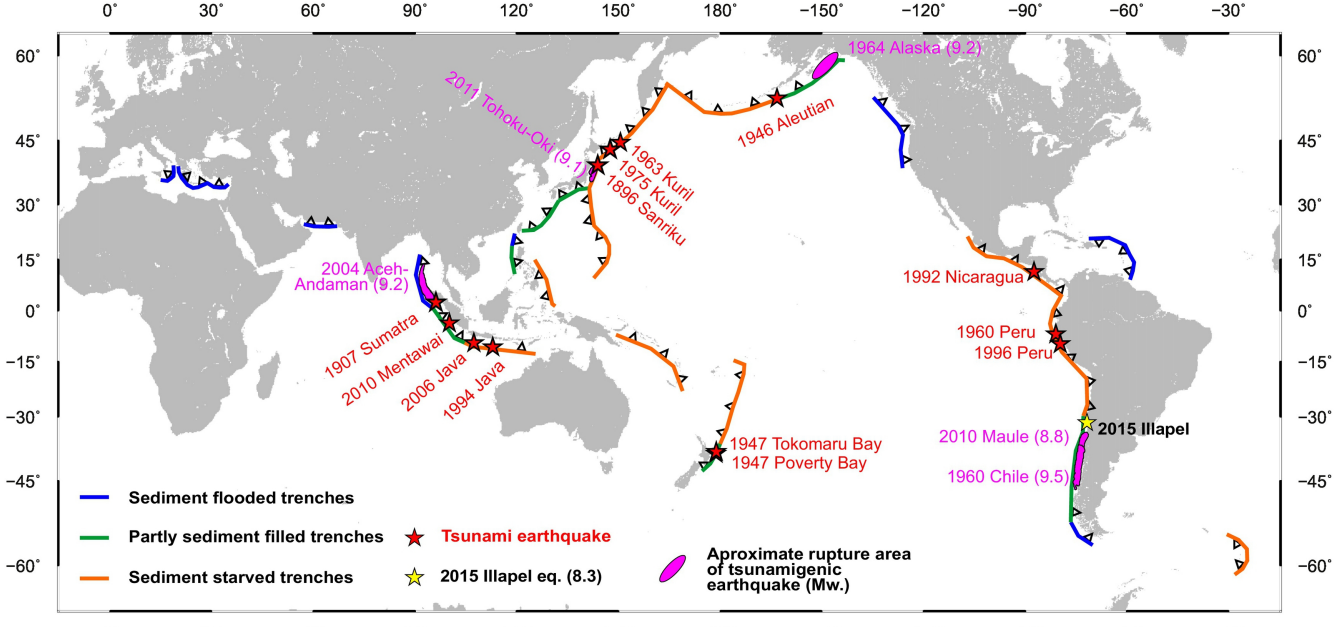
0°
30°
60°
90°
120°
150°
180°
−150°
−120°
−90°
−60°
−30°
60°
45°
30°
15°
0°
−15°
−30°
−45°
−60°
1964 Alaska (9.2)
2011 Tohoku-Oki (9.1)
1946 Aleutian
1963 Kuril
1975 Kuril
1896 Sanriku
2004 Aceh-Andaman (9.2)
1907 Sumatra
2010 Mentawai
2006 Java
1994 Java
1992 Nicaragua
1960 Peru
1996 Peru
2010 Maule (8.8)
2015 Illapel
1960 Chile (9.5)
1947 Tokomaru Bay
1947 Poverty Bay
Sediment flooded trenches
Partly sediment filled trenches
Sediment starved trenches
Tsunami earthquake
2015 Illapel eq. (8.3)
Aproximate rupture area of tsunamigenic earthquake (Mw.)

Figure 9

Sediment starved trenches

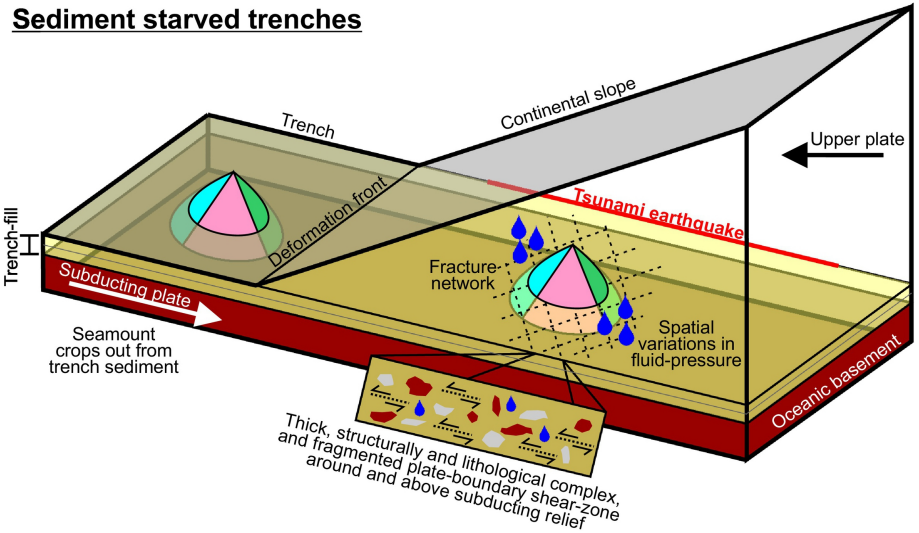

Sediment flooded trenches

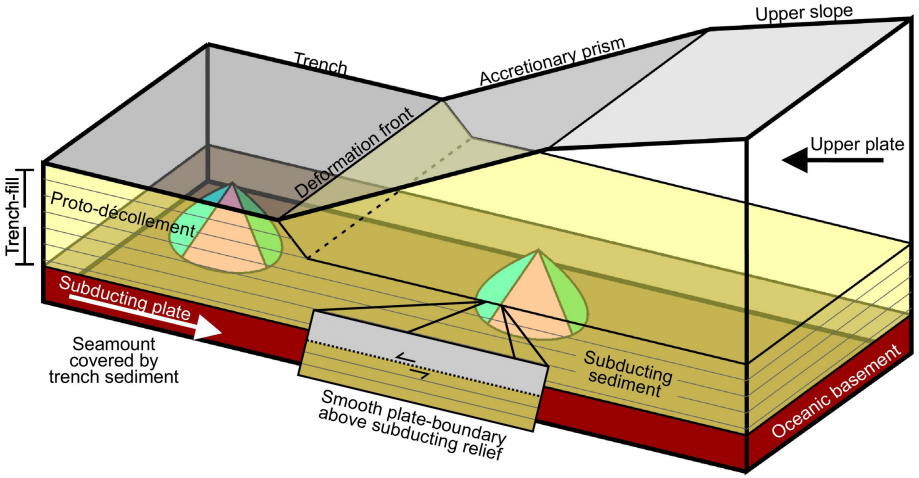

Figure 10